Mon. Not. R. Astron. Soc. **326,** 164–180 (2001)

Luminous and dark matter in the Milky Way

Rob P. Olling[1,2★] and Michael R. Merrifield[3★]

[1]*Department of the Navy, USNO, 3450 Massachusetts Avenue NW, Washington, DC 20392-5420, USA*
[2]*Universities Space Research Association, 300 D Street SW, suite 801, Washington, DC 20024-4703, USA*
[3]*School of Physics and Astronomy, University of Nottingham, University Park, Nottingham NG7 2RD*

Accepted 2001 April 6. Received 2001 March 23; in original form 2000 November 23

ABSTRACT

Axisymmetric models of the Milky Way exhibit strong interrelations between the Galactic constants [the Sun's distance to the Galactic Centre (R_0), and the local rotation speed (Θ_0)], the local stellar column density [$\Sigma_*(R_0)$] and the shortest-to-longest axis ratio of the dark matter halo (q). In this paper we present simple analytical approximations that allow for an efficient search through the vastness of parameter space, and apply this approximation to investigate the consequences of the uncertain gaseous velocity dispersion (σ_g) on the constraints imposed by the thickness of the Milky Way's gas layer. The extra degree of freedom does not significantly alter the conclusions drawn in a previous paper on the shape of the Milky Way's dark matter halo. A significant contribution to the total gas pressure by cosmic rays and magnetic fields beyond the optical disc is thus ruled out. We find that the Milky Way's dark halo is close to spherical if $R_0 \gtrsim 7.1$ kpc, while a significantly flattened dark matter halo is possible only if our distance to the Galactic Centre is smaller than $\sim$6.8 kpc.

Thus, if R_0 is larger than $\sim$7 kpc, or $\Theta_0 \gtrsim 170\,\mathrm{km\,s^{-1}}$, we can rule out two dark matter candidates that require a highly flattened dark matter halo: (1) decaying massive neutrinos, and (2) a disc of cold molecular hydrogen.

It is possible to construct a self-consistent axisymmetric model of the Galaxy based on the IAU-recommended values for the Galactic constants ($R_0 = 8.5$ kpc, $\Theta_0 = 220\,\mathrm{km\,s^{-1}}$) only in the unlikely case that the effective gaseous velocity dispersion is $\sim$19 per cent larger than observed, *and* if the local stellar column density is less than about $18\,\mathrm{M_\odot\,pc^{-2}}$. If we assume that the halo is oblate and a value of Σ_* of $35 \pm 5\,\mathrm{M_\odot\,pc^{-2}}$, we can rule out Galactic models with $R_0 \gtrsim 8.0$ kpc and $\Theta_0 \gtrsim 200\,\mathrm{km\,s^{-1}}$.

Combining the best kinematical and star-count estimates of Σ_*, we conclude that Σ_* probably lies between 25 and $45\,\mathrm{M_\odot\,pc^{-2}}$. We find that Kuijken & Gilmore's determination of the column density of matter within 1.1 kpc of the plane is robust and valid over a wide range of Galactic constants.

Our mass models show that, largely owing to the uncertainty in the Galactic light distribution, the dark matter density in the Galactic Centre is uncertain by up to three orders of magnitude. In the solar neighbourhood this uncertainty is much reduced: our models imply a dark matter density of some $0.42\,\mathrm{GeV}/c^2$ per cubic centimetre, or $(11 \pm 5)\,\mathrm{mM_\odot\,pc^{-3}}$ – roughly 15 per cent of the total mass density.

Key words: Galaxy: fundamental parameters – Galaxy: kinematics and dynamics – solar neighbourhood – Galaxy: stellar content – Galaxy: structure.

1 INTRODUCTION

The observational fact that rotation curves of external galaxies are rather flat in their outer parts (Rubin, Ford & Thonnard 1980; Bosma 1981; Begeman 1987; Kent 1987; Casertano & van Gorkom 1991; Broeils 1992; Persic, Salucci & Stel 1996) indicates the presence of unseen matter in those galaxies.[1] A problem which

★E-mail: olling@usno.navy.mil (RPO); Michael.Merrifield@Nottingham.ac.uk (MRM)

[1] See McGaugh & de Blok (1998) for a review of the alternative hypothesis that the law of gravity has to be modified instead.

is specific for the Milky Way is that we do not know the shape of the Galactic rotation curve (RC). The slope of the RC depends on the assumed values of the Galactic constants (Olling & Merrifield 1998b,c). However, dark matter (DM) is required whatever the values of the Galactic constants. A fit to the observed RC can be used to yield the stellar mass-to-light ratio $\Upsilon_{\rm d}$, and the dark halo parameters, albeit with large uncertainties. Rather than using this fitting procedure, we adopt an analytical approximation in which there is only one free parameter: the degree to which the disc is maximal (γ), from which $\Upsilon_{\rm d}$ and the dark halo parameters follow (see Olling 1995 for details). The parameter γ is preferred for dynamical modelling purposes, as it is bound between 0 and 1 for a zero mass and a full-fledged disc, respectively. For example, in the popular 'maximum-disc' hypothesis (van Albada & Sancisi 1986), the amplitude of the stellar RC equals (85 ± 10) per cent of the observed rotation speed (Sackett 1997), so that $\gamma = 0.85$. In contrast, Bottema (1993) used stellar velocity dispersion measurements to 'weigh' stellar discs, and concluded that they are submaximal, with $\gamma = 0.63 \pm 0.1$. The situation is similarly indeterminate for the Milky Way: the Kuijken & Gilmore (1989a, hereafter KG89a) model implies $\gamma \sim 0.5$, while more recent models with lower rotation speed and shorter scalelengths can be close to maximal ($\gamma = 0.85 \pm 0.1$; Sackett 1997). As a result of the uncertain stellar mass-to-light ratio, the dark halo parameters are very ill-determined for most galaxies (e.g. van Albada & Sancisi 1986; Lake & Feinswog 1989; Olling 1995). The Milky Way is no different: the combined uncertainty in the local disc mass and the stellar scalelength introduces an uncertainty of over three orders of magnitude in the central DM density of the Milky Way, and about an order of magnitude uncertainty in its core radius (Section 2; Dehnen & Binney 1998). In the solar neighbourhood the situation is less dramatic, although no consensus exists on the local volume density of dark matter ($\rho_{\rm DM}$ or the Oort limit; see Section 2 and Crézé et al. 1998 for a recent review). However, the local DM density is important for many astrophysical problems. For example, if the DM comprises elementary particles like neutralinos, axions, neutrinos, gravitinos, etc., their expected detection rate is proportional to the DM density. Likewise, if the dark halo is made up of massive compact halo objects (MACHOs), the event rate for gravitational lensing depends on the integrated DM density along the line of sight towards the lens. Thus, observational signatures of the Milky Way's DM distribution, like microlensing time-scales and optical depths (Gates, Gyuk & Turner 1995), and the expected neutralino annihilation rate (Bergstrom, Ullio & Buckley 1998), depend on the Galactic DM density distribution and hence the assumed values for the Galactic constants.

In a previous paper (Olling & Merrifield 2000, hereafter Paper I) we determined the DM density in the solar neighbourhood[2] at $R = R_0$ and around $R \sim 2R_0$ to infer the minor to major axial ratio ($q = c/a$), or shape, of the DM halo of the Milky Way. In the present paper we investigate the reliability of several of the assumptions made in Paper I, and find that relaxing these assumptions does not greatly change the conclusion of Paper I: the shape of the DM halo of the Milky Way is probably rather round. Before going into more detail, let us review some of the difficulties which arise when one tries to determine $\rho_{\rm DM}$.

First, large values of the local Galactic rotation speed (Θ_0) result in large DM densities, while low rotation speeds require small DM densities. Second, since the *shape* of the Galactic RC depends on the value of our distance to the Galactic Centre (Olling & Merrifield 1998c), the amount of DM increases with R_0 at constant Θ_0. Finally, more highly flattened DM haloes have larger mid-plane densities (Olling 1995).

We use two sets of observations to constrain the mid-plane dark matter density. First, stellar kinematical data provide a measure of the total column density within 1.1 kpc of the plane ($\Sigma_{\rm tot}^{1.1}$; cf. Kuijken & Gilmore 1991, hereafter KG91). The DM density follows after subtracting the luminous components and dividing by the scaleheight. This method yield ambiguous results, because uncertainties in the surface density of stellar matter (Σ_*) translate into a similar uncertainty of the DM density. Thus, low values of Σ_* require more dark matter and hence more highly flattened dark haloes at constant R_0 and Θ_0.

Second, the rate at which the thickness of the gas layer increases with radius ('flaring') is a measure of $\rho_{\rm DM}$. Assuming, for now, a hydrostatic balance between internal pressure and gravity, it follows that an increasing gas layer width is evidence for a decreasing mid-plane density. Large DM densities result in thin gas layers, while low densities yield a thicker gas disc. A larger DM density, due to either a larger Θ_0 and/or R_0 or a smaller q, results in a thinner gas layer. However, such a thinner gas layer would also occur if the actual gas pressure – or, equivalently, the gaseous velocity dispersion, $\sigma_{\rm g}$ – is smaller than assumed: hence the significant correlations between the assumed values of the Galactic constants, Σ_* and $\sigma_{\rm g}$, and the inferred shape of the Milky Way's dark matter halo referred to above.

In practice, the stellar kinematical data impose correlations between Θ_0 and q at the solar circle, while the observed H I flaring does so at $R \sim (2 \pm 0.25)R_0$. At these large radii the stellar disc has vanished, so that the potential is dominated by the gaseous self-gravity and the dark matter.

Unfortunately, the Galactic constants are ill-determined (Kerr & Lynden-Bell 1986; Reid 1993; Olling & Merrifield 1998a; Paper I), and this has consequences for analyses that depend on R_0 and Θ_0. In an ideal world, parameters such as the Galactic constants, the rotation curve [$\Theta(R)$], the scalelength of the optical disc ($h_{\rm d}$), the local stellar column density, the gaseous velocity dispersion, and so forth, are not only measured, but also have normal errors. In that case one could determine quantities that depend on these parameters, such as the DM density or the shape of the halo, by comparing the model and observed parameters in a χ^2 sense. Unfortunately, the quoted errors on R_0 and Θ_0 are not normal, and the values themselves are not averages in the statistical sense, but are rather *consensus* values with *consensus* errors. These arguments lead to the conclusion that the *values* of the Galactic constants and their errors *can not* be used in analyses like maximum-likelihood estimates of a property X which depends on the Galactic constants. Instead, we urge researchers to investigate the dependence of their results on the assumed values of the Galactic constants, and to present their conclusions as functions of R_0 and Θ_0. Given the tremendous increase in computing power, such an approach is currently more feasible than in the past. Practising what we preach, we followed this approach in previous papers (Olling & Merrifield 1998c; Paper I) and will do so in the current article.

In Paper I we used both the constraints set by the flaring of the H I layer as well as the boundary conditions imposed by the local stellar kinematics to infer the halo's flattening. The procedure works as follows: (1) pick values for R_0 and Θ_0, and determine the corresponding RC, (2) create mass models with as ingredients the

[2] Throughout this paper we use cylindrical coordinates with R the Galactocentric distance, and z the distance from the plane.

stellar bulge and disc, the interstellar medium (ISM) and a dark halo of varying degrees of flattening, (3) pick values for the observationally ill-determined scalelength and mass of the stellar disc, (4) select a value for σ_g and calculate model flaring curves (Olling 1995), (5) select the model with flattening $q_{\rm H\,I}$ such that the observed H I flaring at $R \sim 2R_0$ is reproduced (this flattening will be independent of the distribution of the stellar mass), (6) now vary the stellar mass at R_0, (7) keep track of the DM column density $\Sigma_h^{1.1}$ that needs to be added to Σ_* to match $\Sigma_{tot}^{1.1}$, (8) work out which halo flattening $q_{1.1}$ is required to generate $\Sigma_h^{1.1}$, and, finally, (9) select the model that has identical $q_{\rm H\,I}$ and $q_{1.1}$ values. This method is equivalent to finding the zero-point of the $[q_{\rm H\,I}(\Sigma_*) - q_{1.1}(\Sigma_*)]$ function. Graphically, this process can be represented as determining the intersection of the $q_{\rm H\,I}(\Sigma_*)$ and $q_{1.1}(\Sigma_*)$ curves (see Paper I, fig. 3). Note that the $q_{1.1}(\Sigma_*)$ relation hardly depends on the disc scalelength.

In this manner we construct self-consistent mass models, with specific values for h_d, Σ_* and q, for the selected combination of the Galactic constants. Possibly the weakest link in this procedure is the assumed value for σ_g. In the present paper we will remedy this shortcoming of Paper I by repeating the procedure outlined above for many values of the gaseous velocity dispersion. Picking a value for σ_g in the outer Galaxy is related to the question as to the relevance of non-thermal pressure support (due to magnetic fields and cosmic ray energy density) of the gas layer. We investigate these issues in detail in Section 4.

The surface density of stars in the solar neighbourhood provides a significant constraint on the determination of the halo's shape. We therefore review recent determinations in Section 3.1. KG91 claim that the column density within 1.1 kpc of the plane is much better determined than the values of the individual components. However, their Galactic constants lie at the high end of the range we use. Since $\Sigma_{tot}^{1.1}$ provides us with such an important constraint, we consider it prudent to check KG91's assertion. We indeed confirm KG91's finding that $\Sigma_{tot}^{1.1}$ is relatively well determined over a large range in Galactic constants, Σ_* and h_d (Appendix A). In the following section we describe our mass models in more detail, and determine the density of DM in the solar neighbourhood. We summarize and conclude in Section 5.

2 MASS MODELS

In order to interpret the available data, we build axisymmetric Milky Way mass models for which we determine the model values of the total disc mass, the H I flaring, and other parameters. It is well known that the Milky Way deviates from azimuthal symmetry. However, as we have shown in Paper I, and will do so again below, the current observational constraints are only barely good enough to rule out the most extreme combinations of Galactic constants. Thus it would be unrealistic to try to incorporate fine-structure in the stellar mass distribution due to a bar and/or spiral structure, especially since these features are not terribly well determined themselves. This situation may dramatically change with the advent of future astrometric satellites (e.g., *DIVA*, *FAME*, *GAIA*, *SIM*) that could determine the stellar column density over large parts of the Galactic disc.

A comparison between the observations and the models yields the size, mass and shape of the Milky Way. Our models include a stellar bulge and disc, a gas layer, and a dark halo. Some of the relevant parameters of our models are tabulated in Table 1. We consider models with a range of Galactic constants, disc exponential scalelength, stellar disc mass, total column density, and halo flattening. To calculate the *exact* vertical force law $[K_z(R,z)]$ at every point (R, z) in the Galaxy, we integrate over the full mass distribution: $K_z(R,z) = G\int_0^\infty {\rm r}\,{\rm d}r\rho(r,0)\int_{-\infty}^{\infty} {\rm d}w\rho(r,w) \int_{-\pi}^{\pi} \frac{\rm d}{{\rm d}z}\frac{{\rm d}\theta}{|\bar{\mathbf{s}}-\bar{\mathbf{S}}|}$, with $\bar{\mathbf{s}} = \{r, w\}, \bar{\mathbf{S}} = \{R, z\}$, ρ the total mass density at (R, z), and G Newton's constant of gravity (Olling 1995). Since the calculation of K_z and the model flaring curve is rather expensive,[3] we perform these detailed calculations only for the limited subset of models listed in Table 2. We determine the model flaring curves for a much larger range in R_0 and Θ_0 values by applying an approximation (Olling 1995; Appendix D) which we calibrate using the models presented in Table 2; see Section 3.3 for further details.

Table 1. Some parameters used in the model calculations.

bulge:		
d_b	3.53	$L_{\odot,K}\,pc^{-3}$
q_b	0.61	
h_b	667	pc
ζ_b	10	pc
$\rho_b(0)$	15.24	$L_{\odot,K}\,pc^{-3}$
$L_{b,K,tot}$	1.5×10^{10}	$L_{\odot,K}$
disc:		
z_e	300	pc
h_d	2, 2.5, 3	kpc
$L_{d,K}(0)$	2200, 1408, 978	$L_{\odot,K}\,pc^{-2}$ ($h_d = 2, 2.5, 3$)
$\Sigma_*(R_0)$	25–45	$L_\odot\,pc^{-2}$
ρ_*	26.5–47.7	$10^{-3}\,M_\odot\,pc^{-3}$
$L_{d,K,tot}$	$5.5\ 10^{10}$	$L_{\odot,K}$
ISM at R_0:		
$\Sigma_{\rm H\,I+H\,II}$	9.25	$M_\odot\,pc^{-2}$
Σ_{H_2}	1.80	$M_\odot\,pc^{-2}$
$FWHM_{\rm H\,I}$	410 ± 30	$(R_0/7.1)$ pc
$FWHM_{H_2}$	141 ± 20	$(R_0/7.1)$ pc
$\rho_{\rm H\,I+H\,II}$	21 ± 1.5	$(7.1/R_0)\ 10^{-3}\,M_\odot\,pc^{-3}$
ρ_{H_2}	12 ± 1.5	$(7.1/R_0)\ 10^{-3}\,M_\odot\,pc^{-3}$
$\rho_{\rm ISM}$	43 ± 3.0	$(7.1/R_0)\ 10^{-3}\,M_\odot\,pc^{-3}$

2.1 The mass components

2.1.1 *Stellar components*

We base our model for the bulge on Kent's (1992) K-band luminosity distribution. The bulge is a modified spheroid with 'boxy' appearance and density: $\rho_b(s) = d_b K_0(s/h_b)$, with $s^4 = R^4 + (z/q_b)^4 + \zeta_b^4$. The bulge is flattened, with axial ratio q_b. To avoid the singularity of the K_0-Bessel function at $s = 0$, we include a softening ζ_b. We also truncate the bulge exponentially beyond 3 kpc.

For the disc, we use the standard form of a radially exponential disc with central K-band surface brightness $L_{d,K}(0)$ and scalelength h_d. We will consider models with values for the scalelength that are considered to be reasonable (Sackett 1997). Furthermore, we use the observational fact that the total luminosity is better determined than either the central surface brightness or the scalelength (Kent, Dame & Fazio 1991). Thus we scale $L_{d,K}(0)$ such that the total

[3] The calculation of model gas layer widths for a given combination of R_0, Θ_0, h_d and bulge and disc mass-to-light ratios takes about 1.3 hours per q-value, on a SPARC-10 processor.

Table 2. Disc and halo parameters. A log for a representative sample of models for which *exact* flaring curves are calculated. The meaning of the columns is as follows: (1) γ, the degree to which the stellar disc is maximal; (2) scalelength of stellar disc (kpc); (3) and (4) bulge and disc K-band mass-to-light ratios; (5) and (6) stellar column density and total column density within 1.1 kpc of the plane ($M_\odot\,pc^{-2}$); (7) and (8) core radius (kpc) and central density ($m\,M_\odot\,pc^{-3}$) of the dark halo, assuming $q = 1$ (multiply by $\approx 1/q$ to scale to different values of q; for a more exact scaling see Olling 1995); (9) and (10) dark halo flattening as inferred from the H I flaring ($q_{\rm H\,I}$) and the local columndensities ($q_{1.1}$). For a given set of (R_0, Θ_0, $h_{\rm d}$), the $q_{\rm H\,I}$ errors for the Milky Way are similar to those for extragalactic systems (Olling 1996a).

γ	$h_{\rm d}$	$\Upsilon_{\rm b,K}$	$\Upsilon_{\rm d,K}$	Σ_*	$\Sigma_{\rm tot}^{1.1}$	$R_{\rm c}$	$\rho_0(q=1)$	$q_{\rm H\,I}$	$q_{1.1}$
$R_0 = 6.8$,	$\Theta_0 = 182$								
0.80	2.0	0.55	0.422	30.21	62.48	2.39	73.8	0.630 ± 0.107	0.561 ± 0.175
0.86	2.0	0.55	0.488	34.92	66.02	3.54	35.6	0.687 ± 0.113	0.664 ± 0.226
0.92	2.0	0.55	0.558	39.96	68.72	6.09	14.6	0.699 ± 0.120	0.753 ± 0.295
0.64	2.5	0.55	0.327	29.58	63.56	1.32	246.3	0.687 ± 0.152	0.620 ± 0.183
0.70	2.5	0.55	0.392	35.39	68.84	1.86	125.1	0.717 ± 0.134	0.826 ± 0.268
0.75	2.5	0.55	0.449	40.63	73.40	2.45	73.0	0.674 ± 0.127	1.061 ± 0.371
0.56	3.0	0.55	0.306	30.21	64.34	0.70	853.9	0.740 ± 0.181	0.651 ± 0.194
0.60	3.0	0.55	0.351	34.68	68.6	1.00	421.0	0.770 ± 0.159	0.820 ± 0.261
0.65	3.0	0.55	0.412	40.70	74.18	1.44	201.9	0.762 ± 0.137	1.114 ± 0.382
$R_0 = 7.1$,	$\Theta_0 = 189$								
0.82	2.0	0.45	0.482	29.71	61.94	2.73	62.7	0.625 ± 0.132	0.544 ± 0.165
0.89	2.0	0.45	0.568	35.00	65.66	4.53	25.5	0.624 ± 0.116	0.636 ± 0.214
0.95	2.0	0.45	0.647	39.87	66.74	9.77	8.6	0.679 ± 0.104	0.603 ± 0.239
0.65	2.5	0.55	0.370	29.66	62.60	1.13	340.1	0.727 ± 0.159	0.581 ± 0.173
0.71	2.5	0.55	0.441	35.39	67.76	1.66	158.2	0.738 ± 0.161	0.765 ± 0.250
0.76	2.5	0.55	0.506	40.55	72.26	2.25	86.4	0.823 ± 0.223	0.999 ± 0.356
0.56	3.0	0.55	0.333	29.73	61.82	0.20	9884.5	0.735 ± 0.181	0.550 ± 0.168
0.61	3.0	0.55	0.395	35.28	67.10	0.55	1343.6	0.703 ± 0.158	0.734 ± 0.243
0.63	3.0	0.55	0.421	37.63	69.32	0.71	802.8	0.786 ± 0.210	0.843 ± 0.290
$R_0 = 7.8$,	$\Theta_0 = 207$								
0.92	2.0	0.45	0.687	29.80	64.60	9.51	15.4	1.003 ± 0.119	0.616 ± 0.162
0.72	2.5	0.75	0.492	29.80	64.76	4.59	47.9	1.744 ± 0.553	0.963 ± 0.240
0.78	2.5	0.75	0.577	34.97	71.00	5.81	32.6	1.616 ± 0.443	1.065 ± 0.260
0.84	2.5	0.75	0.669	40.56	77.66	8.01	20.6	1.461 ± 0.337	1.191 ± 0.331
0.59	3.0	0.75	0.430	30.46	66.54	2.84	103.4	1.623 ± 0.451	0.973 ± 0.244
0.61	3.0	0.75	0.460	32.56	68.06	3.02	91.7	2.019 ± 0.758	1.026 ± 0.260
0.68	3.0	0.75	0.572	40.46	77.54	3.81	59.3	1.810 ± 0.753	1.327 ± 0.364
$R_0 = 8.5$,	$\Theta_0 = 227$								
0.76	2.5	0.60	0.670	30.66	78.68	6.81	39.1	2.922 ± 0.863	1.169 ± 0.252
0.81	2.5	0.60	0.761	34.83	80.43	8.34	28.9	2.512 ± 0.608	1.228 ± 0.279
0.86	2.5	0.60	0.857	39.26	81.28	11.10	19.9	1.931 ± 0.366	1.256 ± 0.306
0.59	3.0	0.85	0.486	27.23	76.53	5.09	60.2	1.424 ± 0.156	1.165 ± 0.193
0.67	3.0	0.85	0.627	35.11	82.49	6.20	43.2	1.498 ± 0.183	1.364 ± 0.213
0.75	3.0	0.85	0.785	44.00	88.53	8.07	28.9	1.475 ± 0.197	1.641 ± 0.159

luminosity is conserved for each choice of $h_{\rm d}$. However, the numerical values of $L_{{\rm d},K}(0)$ and $h_{\rm d}$ depend on our choice of R_0. From Freudenreich (1996, 1998) we find that these quantities typically increase with R_0, by 8 per cent $\times$ (R_0/kpc $-$ 8). Such variations induce a change in total luminosity which is 3 times larger. However, because these corrections are smaller than the changes resulting from the uncertainty in $h_{\rm d}$, we do not scale $L_{{\rm d},K,{\rm tot}}$ with R_0. For the disc's vertical distribution we use a secant-hyperbolic function [sech($z/2\times z_{\rm e}$)], which is a compromise between the often-used exponential and secant-hyperbolic-squared forms (van der Kruit 1988). For simplicity, the exponential scale-height ($z_{\rm e}$) of the disc is taken to be constant at 300 pc, intermediate between the values suggested by Kent (1992) and Reid & Majewski (1993). However, note that our results depend neither on $z_{\rm e}$ nor on the particularities of the vertical density distribution. We use disc mass-to-light ratios ($\Upsilon_{{\rm d},K}$) such that the Kuijken & Gilmore (1989, hereafter KG89b) 2σ range for the local stellar column density is spanned. The stellar disc is truncated at ($R_0 + 4.5$) kpc (Robin, Crézé & Mohan 1992; Freudenreich 1996, 1998).

2.1.2 *Interstellar medium components*

We now turn to the contribution to the mass models from the ISM. Our location inside the Milky Way means that distances to diffuse components like the ISM are based on a kinematical model. Thus, important properties like the full-width at half-maximum (FWHM), volume density, and total mass of the ISM depend on the Galactic constants and the RC of the Milky Way. Thus we redetermine the atomic and molecular gas distributions for each

choice of R_0 and Θ_0. While the columndensities at *fractional radius* R/R_0 are independent[4] of the choice of R_0 and Θ_0, the number density, the thickness and the total gas mass of the Galaxy are not. Observationally, we can currently do no better than determining the gaseous column density (Σ_g) at fractional radius R/R_0. Likewise, since the thickness measurement returns an angular size, we can only determine FWHM/R_0 at fractional radius R/R_0 [FWHM/$R_0 = \zeta R/R_0$ (Binney & Merrifield 1998), their fig. 9.25]. Physical length-scales for the thickness and Galactocentric radius can be assigned after choosing a value for R_0.

For the inner Galaxy, the H I column density was determined from the mid-plane volume density (Burton 1988) and the observed thickness of the layer (Malhotra 1995). The H I columndensities for $R \gtrsim R_0$ were taken from Wouterloot et al. (1990). The H_2 columndensities for the inner and outer Galaxy were copied from Bronfman et al. (1988) and Wouterloot et al. (1990), respectively.[5] For the radial profiles of the ISM we neglect the column density due to the other phases of the ISM. However, in order to properly take into account all baryonic contributions to the local column density, we include $1.4\,M_\odot\,pc^{-2}$ of ionized hydrogen (Kulkarni & Heiles 1988) *at the solar position only*. We further include 23.8 per cent helium by mass (Olive & Steigman 1995) to compute the surface densities.

As in our previous papers, we do not distinguish between the various phases of the atomic hydrogen, but rather assume that the warm neutral medium has a kinetic temperature equivalent to the 'temperature' associated with the bulk motions of the clumped, cold neutral medium. Note that the cold medium is likely to be absent beyond the stellar disc (Braun 1997; Paper I).

2.1.3 *The dark matter component*

As is commonly done (e.g. van Albada & Sancisi 1986; Kent 1987; Begeman 1989; Lake & Feinswog 1989; Sackett & Sparke 1990; Broeils 1992; Olling 1995; Olling 1996b), we model the DM density distribution as a non-singular isothermal spheroid with flattening q, and a density distribution given by

$$\rho_h(R,z;q) = \rho_0(q)\left[\frac{R_c^2(q)}{R_c^2(q) + R^2 + (z/q)^2}\right], \qquad (1)$$

where the halo's core radius (R_c) and central density (ρ_0) depend on the flattening in such a way that the family of density distributions $\rho_h(q)$ have a rotation curve that is essentially independent of q (Olling 1995). Fig. 1 shows the radial distribution of dark matter

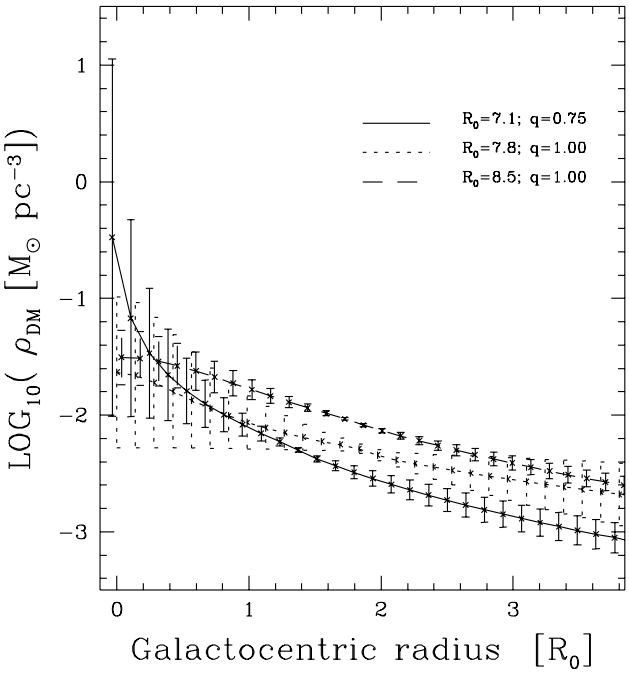

Figure 1. The dark matter mid-plane density distribution calculated using equation (1) for three values of R_0 and q. The densities scale approximately as $1/q$ (Olling 1995) The error bars represent the full range for the case corresponding to $\Sigma_* = 35 \pm 5\,M_\odot\,pc^{-2}$, and $h_d = 2$ to 3 kpc. Notice that although the DM density at the solar circle is relatively well determined, the central density is uncertain by more than three orders of magnitude. Note that we have offset the radial coordinates of the $R_0 = 7.1$, and 8.5 kpc models from their true positions (i.e., the $R_0 = 7.8$ kpc points) to avoid overlapping symbols.

for three values of R_0, for the range in model parameters as listed in Table 2. Each choice for h_d and Σ_* results in a different distribution. The largest DM densities are obtained for large h_d and small Σ_* values. Even though the central DM density is uncertain by over three orders of magnitude, the local DM density is determined rather well; we find:

$$\frac{\rho_{DM}(R_0,\Theta_0)}{10^{-3}\,M_\odot\,pc^{-3}} = \frac{11.5 + 3.8\times(R_0 - 7.8) \pm 2}{q(26.7/\Omega_0)^2}, \qquad (2)$$

with $\Omega_0 = \Theta_0/R_0$, and where R_0 is in kpc, and Θ_0 in $km\,s^{-1}$. The ($\sim 25/q$) per cent uncertainty arises as a result of the uncertainty in $\Sigma_{tot}^{1.1}$ and Σ_*. For example, taking $R_0 = 7.1$ kpc and $q = 0.71$, and using the parameters tabulated in Table 2, we find $\rho_{DM}(R_0) = 10.5\,m\,M_\odot\,pc^{-3}$ ($1\,mM_\odot\,pc^{-3} = 10^{-3}\,M_\odot\,pc^{-3}$). Thus the $R_0 = 7.1$ model value for the DM density compares well with the values given by equation (2), as well as with the observational determination (Section 3.1).

2.2 Other dark matter models

Of course, other mass models can be constructed which represent the radial DM density distribution (e.g. van Albada & Sancisi 1986; Navarro, Frenk & White 1996; Dehnen & Binney 1998). However, all viable mass models must share the property that they reproduce the Galactic RC. For a round halo the vertical force approximately equals z/R times the radial force. Since the radial force is approximately the same for all models which reproduce the observed RC, the ensemble of possible models also have

[4] From Binney & Merrifield's (1998) equation 9.12 it follows that the distance-dependent function that appears in the exponential term depends only on $r = R/R_0$, so that one can rewrite the observed brightness temperature at line-of-sight velocity u_{los} as $R_0 \int dr F(r,\ldots) n(r)\, H(u_{los}, r, \ldots)$, with F a function that results from the transformation from line-of-sight distance to r, and H the velocity-dependent function. If H varies more quickly with r than the number density $n(r)$, then the product $R_0 \times n(r)$ is approximately constant. Thus, as R_0 is increased, the volume density goes down. Because the gas-layer width *increases* with R_0, the vertical column density at scaled distance R/R_0 is *independent* of the Galactic constants. See also Bronfman et al. (1988).

[5] A graphical representation of the derived gaseous surface density distributions can be found in a related paper on the Galactic and Oort constants (Olling & Merrifield 1998c). The H_2 columndensities have been rescaled from the original sources, assuming $N(H_2)/W(CO) = 2.3 \times 10^{20}\,cm^{-2}(K\,km\,s^{-1})^{-1}$. We present the radial increase of the thickness of the gas layer in Paper I. The thickness and column density of the H I and H_2 are tabulated in Appendix D.

approximately equal vertical forces, independent of the exact radial DM density distribution (Olling 1995). In a flattened halo with the same RC, the DM densities are roughly proportional to $1/q$, independent of the radial mass distribution (cf. equation 2). Thus our analysis will not be seriously compromised by restricting ourselves to one particular DM density distribution.

3 CONSTRAINING THE DARK MATTER DENSITY

In this section we present two simple analytical models to illustrate the existing correlations between R_0, Θ_0, $\Sigma_{\rm tot}^{1.1}$, Σ_*, q and $\sigma_{\rm g}$ outlined in the Introduction. These models can be used to show how the local stellar kinematics and the H I flaring constrain the dark matter density in the solar neighbourhood and at $\sim 2\ R_0$. However, first we investigate how well the local stellar column density is determined, and how accurately this determination constrains the DM density in the solar neighbourhood.

3.1 The local stellar column density: a constraint?

The Milky Way is a unique galaxy in that we can, at least in principle, determine the local column density of stars directly. Once Σ_* is accurately determined, it is possible to establish to what degree the Milky Way disc is maximal, which would provide an important benchmark for external galaxies. Unfortunately, this benchmark is not yet available, as the values for Σ_* reported in the literature range from 26 to $145\,{\rm M}_\odot\,{\rm pc}^{-2}$.

Two basic techniques have been employed to determine Σ_*. The direct method involves converting star counts as a function of Galactic coordinates and magnitude to in situ mass densities. This method is somewhat hampered by uncertainties in the conversion from luminosity to mass, completeness problems in the solar circle neighbourhood, and binary corrections at large distances. Gould, Bahcall & Flynn (1997, hereafter GBF97) used deep *HST* star counts of M dwarfs at great heights above the plane, in combination with a local normalization to infer a stellar column density of only $25.8 \pm 3.8\,{\rm M}_\odot\,{\rm pc}^{-2}$. The second, kinematical, method employs the interrelationship between the potential, the vertical density distribution, and the variation of the velocity dispersion with z. Many authors have employed this method, yielding a large range in inferred values for Σ_*. For example, Bahcall (1984b) found that the inferred value of Σ_* depends significantly on the assumed vertical distribution of the dark matter: $\sim$40, $\sim$52, $\sim$68, and $\sim 145\,{\rm M}_\odot\,{\rm pc}^{-2}$ for DM distributions that resemble the gaseous disc, an isothermal halo, the thin stellar disc, or the thick stellar disc, respectively. Other authors find values as low as $35\,{\rm M}_\odot\,{\rm pc}^{-2}$ (KG89b; Flynn & Fuchs 1994). Methods that combine the two primary methods exist as well (Bienaymé, Robin & Crézé 1987; Crézé, Robin & Bienaymé 1989). In Appendix A we simulate the kinematic determination of the stellar column density with the aid of Galaxy models – taken from Table 2 – for which we know the exact force law. Our results are in complete agreement with the findings of previous authors: the 'vertical disc–halo conspiracy' can only be resolved if high-z stellar kinematical data are included and/or if additional assumptions are made (e.g., a 'reasonable' value for the DM density). Typical values for the mass of the *stellar* disc are 52 (Bahcall 1984b), 35 ± 5 (KG89b) and $37 \pm 13\,{\rm M}_\odot\,{\rm pc}^{-2}$ (Flynn & Fuchs 1994).

Considering the uncertainties in the kinematical estimates of the total mass of the disc, it might be preferable to use the direct star count method to determine Σ_*. The latest results by GBF97 imply $\Sigma_* = 25.8 \pm 3.8\,{\rm M}_\odot\,{\rm pc}^{-2}$. However, the local space density of stars found by these authors, $(33.2 \pm 8.6)\,{\rm m\,M}_\odot\,{\rm pc}^{-3}$ is somewhat lower than the values reported in the literature, $43 \pm 15\,{\rm m\,M}_\odot\,{\rm pc}^{-3}$.[6] This suggests that GBF97 may have underestimated Σ_* by a factor of 1.4 ± 0.2, and so we find $\Sigma_* = 36 \pm 5\,{\rm M}_\odot\,{\rm pc}^{-2}$: the star count method yields a value for Σ_* that is remarkably close to the kinematical estimates.

On the other hand, the total matter density in the solar neighbourhood as inferred from recent *Hipparcos* data (Crézé et al. 1998) of $76 \pm 15\,{\rm m\,M}_\odot\,{\rm pc}^{-3}$ favours a local stellar volume density which is even smaller than reported by GBF97. After subtracting the density of the ISM (see Table 1) and the local DM density (equation 2), we find a local stellar density of $\sim 21 \pm 15\,{\rm m\,M}_\odot\,{\rm pc}^{-3}$. Note that even lower values for ρ_* result if large values for the Galactic constants and/or Ω_0 are chosen, while smallish Galactic constants and Ω_0 *increase* the local stellar density.

To summarize, a 'reasonable' value for Σ_* might be $35\,{\rm M}_\odot\,{\rm pc}^{-2}$, and we suggest a 'consensus' error of $10\,{\rm M}_\odot\,{\rm pc}^{-2}$. However, since the differences between the various Σ_* estimates are not random but systematic, one *should not* interpret the reasonable Σ_* value and its error in a statistical sense. That is to say, *one can not construct likelihood contours based on a reasonable average value and a consensus error bar.* Any attempt to do so would be an overinterpretation of the available data.

A 'reasonable' value for the local dark matter column can be obtained by subtracting the columndensities of the stellar and ISM distributions: $\Sigma_{\rm h} = (24.5 \pm 11)\,{\rm M}_\odot\,{\rm pc}^{-2}$ within 1.1 kpc of the plane. This DM column amounts to an average local DM density of $11 \pm 5\,{\rm m\,M}_\odot\,{\rm pc}^{-3}$.

3.2 The connection between dark and luminous matter in the solar neighbourhood

In the previous section we have seen that the contribution of the stellar and DM components to the local disc mass cannot be clearly segregated. Thus the observed value for $\Sigma_{\rm tot}^{1.1}$ implies that Σ_* and $\Sigma_{\rm h}$ are highly correlated: a low stellar column implies a large amount of DM, and vice versa. Since the DM density depends on the amplitude of the RC and the halo's flattening, these parameters are in turn related to Σ_*. Below we investigate the relations between $\Sigma_{\rm tot}^{1.1}$, Θ_0, Σ_* and q in some detail. These relations are independent of the H I flaring.

Integrating equation (1) with respect to z and applying equation (A4) from Olling (1995), we find the column density of DM within z of the Galactic plane as a function of q:

$$\Sigma_{\rm h}^{z}(q) = \frac{2q\rho_0(q)R_{\rm c}^2(q)}{\sqrt{R_{\rm c}^2(q)+R^2}} \arctan\left[\frac{z/q}{\sqrt{R_{\rm c}^2(q)+R^2}}\right] \tag{3}$$

$$= \frac{V_{\rm h,\infty}^2\sqrt{1-q^2}}{2\pi G\sqrt{R_{\rm c}^2(q)+R^2}\arccos q} \arctan\left[\frac{z/q}{\sqrt{R_{\rm c}^2(q)+R^2}}\right], \tag{4}$$

with $V_{\rm h,\infty}$ the asymptotic rotation velocity of the round dark halo.

[6] The average of $\rho_* = 46$ (Wielen 1974), 50.8 (Bahcall 1984a; Bahcall, Flynn & Gould 1992) and $45\,{\rm m\,M}_\odot\,{\rm pc}^{-3}$ (Crézé et al. 1998).

For each of our self-consistent mass models we can calculate $\Sigma^{1.1}_{\rm tot}(q)$, and we find that it obeys a simple power-law relation:

$$\Sigma^{1.1}_{\rm tot}(q) = \Sigma^{1.1}_{\rm h}(q) + \Sigma_* + \Sigma_{\rm g} \tag{5}$$

$$\approx \Sigma^{1.1}_{\rm tot}(q=1) \times q^{-p}. \tag{6}$$

The dependence of $\Sigma^{1.1}_{\rm tot}$ on the other parameters of the model parameters are combined into the index p (with $p \sim 0.05$–0.45).[7] The halo flattening inferred from the local stellar kinematics ($q_{1.1}$) is then found by equating $\Sigma^{1.1}_{\rm tot}(q)$ with the observed value and solving equation (6) for q:

$$q_{1.1} = \left[\frac{\Sigma^{1.1}_{\rm tot}(q=1)}{71 \pm 6}\right]^{1/p}. \tag{7}$$

Equations (4), (6) and (7) can be combined to find the dependence of $q_{1.1}$ on the Galactic constants. Neglecting $R_{\rm c}$ and equating $V_{\rm h,\infty}$ with Θ_0, we find:

$$q_{1.1} \propto \left(\frac{c\Theta_0^2/R_0^2 + \Sigma_* + \Sigma_{\rm g}}{\Sigma^{1.1}_{\rm tot}}\right)^{1/p}, \tag{8}$$

where c is a constant. Qualitatively, this is the functional dependence we expect: increasing Θ_0 at constant R_0 would increase the required amount of DM, which has to be counteracted by increasing $q_{1.1}$ to retain the same $\Sigma^{1.1}_{\rm tot}$. Likewise, increasing R_0 would place the Sun in a lower density region of the halo, which needs to be compensated by decreasing $q_{1.1}$. Furthermore, given the small values of p, $q_{1.1}$ depends very strongly upon the Galactic constants.

In Appendix B we present some other correlations between the Galactic constants, Σ_*, Θ_0 and $q_{1.1}$. For example, equation (B4) reveals the linear relation between $q_{1.1}$ and Σ_* for $q \gtrsim 0.15$. Note that models with different scalelengths follow the same $q_{1.1}(\Sigma_*)$ relation, albeit that different $h_{\rm d}$s yield different $q_{1.1}$s for a given stellar column density.[8] These examples show that the $\Sigma^{1.1}_{\rm tot}$ constraint implies highly flattened DM haloes for small values of Θ_0.

3.3 Constraints from the thickness of the gas layer

In an idealized picture, the equilibrium thickness of the gas in the Milky Way depends only on the gas 'temperature' and the form of the potential in which it has settled. Thus the observed FWHM of the gas layer can be used to constrain the potential of the Galaxy. In Paper I we present evidence that the ISM beyond the optical disc comprises only a single, isothermal component. We therefore adopt the same assumption in the analysis below. In this section we will expand our analysis to include the effects of non-thermal pressure gradients.

If the gas layer is in a steady state and we assume that only 'thermal' motions of the gas contribute to the pressure in the ISM, the thickness of the gas layer follows from the equation of hydrostatic equilibrium:

$$\frac{{\rm d}\sigma_{\rm g}^2\rho_{\rm g}(z)}{{\rm d}z} = \rho_{\rm g}(z)K_z(z), \tag{9}$$

where $\sigma_{\rm g}$, $\rho_{\rm g}(z)$, and K_z are the gaseous velocity dispersion and volume density, and the vertical force per unit mass, respectively. The vertical force is commonly determined using a 'local approximation' where K_z follows from the Poisson equation, and the local mass densities and the radial gradient of the RC. However, this approach is known to fail in regions where either the mass densities or the rotation curve, or both, have steep gradients. Further, the local approach neglects any variation of the circular speed with height above the plane. These problems can be overcome by calculating K_z from the global mass distribution (the 'global approach,'; Olling 1995). As mentioned in Section 2, we combine the exactness of the global approach with the speed of the local approximation for optimal results.

If we employ the local approximation the dependencies between the various parameters of the model become apparent. For example, when the potential is dominated by mass component i, equation (9) can be solved for the thickness of the gas layer:

$${\rm FWHM_i} \propto \frac{\sigma_{\rm g}}{\sqrt{4\pi G\rho_i}}, \tag{10}$$

where the proportionality constant depends on the vertical density distribution of the dominant contributor to the local vertical potential. We copy some relations from Olling (1995). In case the gas is fully self-gravitating, the width is given by

$${\rm FWHM_g} \approx 0.158\frac{\sigma_{\rm g}^2}{\Sigma_{\rm g}}. \tag{11}$$

If the potential is dominated by an isothermal stellar disc with sech^2 scale-height z_0 ($z_0 = 2z_{\rm e}$), the thickness of a gas layer would be

$${\rm FWHM_*} \approx 0.51\sigma_{\rm g9.2}\sqrt{\frac{z_{0,0.6}}{\Sigma_{*35}}}. \tag{12}$$

or 510 pc at the solar circle ($\sigma_{\rm g}$, z_0 and Σ_* are expressed in units of 9.2 km s^{-1}, 0.6 kpc and 35 M$_\odot$ pc^{-2}; see also van der Kruit 1988). Also, if the DM halo dominates the potential, we find:

$${\rm FWHM_h} \approx \sqrt{\frac{13.5q}{1.4+q}}\frac{\sigma_{\rm g}}{V_{\rm h,\infty}}\sqrt{R_{\rm c,1}^2 + R^2}, \tag{13}$$

where $R_{\rm c,1}$ is the core radius of the equivalent round halo (Olling 1995). All distances and widths are in kpc, and all velocities in km s^{-1}. The thickness of the gas layer in the combined potential of several mass components can be solved analytically in the form of an integral equation, but requires an iterative solution procedure (Olling 1995; Appendix C). However, a further approximation is possible. Following Olling (1995; Appendix D) we use

$$\frac{1}{{\rm FWHM_g^2}} \approx \sum_i \frac{w_i}{{\rm FWHM_i^2}}, \tag{14}$$

where the weighting factors w_i reflect the relative importance of component i in the region where the gas resides.[9] Solving equation

[7] The values for $\Sigma^{1.1}_{\rm tot}(q)$, $\Sigma^{1.1}_{\rm tot}(q=1)$ and p are different for each combination of the Galactic constants, the stellar disc mass and scalelength. p can be determined from a fit to equation (6), where we determine $\Sigma^{1.1}_{\rm tot}(q)$ for several models with varying qs. Note that we also use equation (6) to extrapolate into the prolate regime, with the exponent p as determined for the oblate models.

[8] The reader can verify this by plotting the $q_{1.1}$ values as a function of Σ_* from Table 2.

[9] See Olling (1995) for details. For the Milky Way we use: $w_{\rm g} = [1.24\Sigma_{\rm g} + 1.55W_{\rm h} \times (\rho_{\rm h} + \rho_{\rm r})/[\Sigma_{\rm g} + W_{\rm h} \times (\rho_{\rm h} + \rho_{\rm r})]$, $w_{\rm h} = [1.0 + 0.35 \times \exp(-1.7W_{\rm h}\rho_{\rm h}/\Sigma_{\rm g})]$, and $w_{\rm r} = (1 + w_{\rm h})/2$. $\rho_{\rm h}$ is the local dark matter density, the 'rotational' density, $\rho_{\rm r}\left(\equiv \frac{-1}{2\pi G}\frac{V_{\rm rot}}{R}\frac{{\rm d}V_{\rm rot}}{{\rm d}R}\right)$, arises due to the slope of the rotation curve. $W_{\rm h}$ equals FWHM$_{\rm h}$/2.35. For example, at R $\sim 2R_0$, $\Sigma_{\rm g} \sim 7.7$ and $(\Sigma_{\rm h}, \Sigma_{\rm r}) = (3.6, -0.30), (5.3, -0.17)$ and $(6.0, -0.37)$ M$_\odot$ pc^{-2} for $R_0 = 7.1$, 7.8 and 8.5 kpc, respectively. These values lead to weights that are almost independent of R_0: $w_{\rm g} \sim 1.4$, $w_{\rm h} \sim 1.2$ and $w_{\rm r} \sim 1.1$. These weightings embody the calibration of the local approximation for the outer Milky Way.

(14) for $q_{\rm H\,I}$, taking $V_{\rm h,\infty} \approx \Theta_0$ and neglecting $R_{\rm c,1}$, we find:

$$q_{\rm H\,I}(2R_0) \approx \frac{1.4}{13.5\left[\frac{1}{w_{\rm h}}\left(\frac{\sigma_{\rm g}}{\zeta\Theta_0}\right)^2 - \frac{w_{\rm g}}{w_{\rm h}}\left(\frac{\Sigma_*}{0.159\sigma_{\rm g}}\frac{2R_0}{\Theta_0}\right)^2\right] - 1}, \quad (15)$$

with $\zeta(R) = {\rm FWHM_{obs}}/R$ ($\sim$0.07 for the outer Milky Way), and where $\Sigma_{\rm g}$, $w_{\rm g}$ and $w_{\rm h}$ have to be evaluated at $R = 2R_0$. From this equation we infer that the contribution of the self-gravity of the gas depends strongly on the gaseous velocity dispersion: low $\sigma_{\rm g}$ values result in a more negative self-gravity contribution to the denominator, and hence lead to a larger inferred $q_{\rm H\,I}$. As we have already mentioned, the self-gravity of the gas is an important component, as it reduces the width of the gas layer by approximately 45 per cent. A further simplification can be made by neglecting the gaseous self-gravity and setting $w_{\rm h}$ to unity:

$$q_{\rm H\,I} \approx \frac{1.4[\zeta(R)\Theta_0]^2}{13.5\sigma_{\rm g}^2 - [\zeta(R)\Theta_0]^2}, \quad (16)$$

$$q_{\rm H\,I} \propto \frac{\Theta_0^2}{\sigma_{\rm g}^2}, \quad (17)$$

where the second line arises because the first term in the denominator dominates. The errors in the halo flattening and rotation speed are related through equation (C1), where we have neglected the contribution of the velocity dispersion error. The dependence of $q_{\rm H\,I}$ on Θ_0 and $\sigma_{\rm g}$ are indeed as outlined in the Introduction. Also note that, due to the quadratic nature of the proportionalities, the observed flaring and the small allowed range of $q_{\rm H\,I}$ constrain Θ_0 and $\sigma_{\rm g}$ rather tightly.

Comparing equations (8) and (17), we see that the constraints on the halo shape arising from the local stellar kinematics and the H I flaring have rather different R_0 and Θ_0 dependencies. Thus it is indeed possible to learn more about the Galactic DM distribution by combining these two constraints. Further, unlike the stellar kinematical method, the constraints from the H I flaring is independent of Σ_*, since it arises at $R \sim 2R_0$, beyond the truncation of the stellar disc.

Equations (15)–(17) serve *only* to illustrate the dependence of $q_{\rm H\,I}$ on the model parameters, since several important aspects are treated too simplistic. First, neglecting $R_{\rm c}$ and equating $V_{\rm h,\infty}$ with Θ_0 is only seldomly warranted. Second, depending on the slope of the rotation curve, an error of order $\pm$20 is made in the inferred $q_{\rm H\,I}$. We therefore do not recommend using equations (15)–(17) 'as is' to determine $q_{\rm H\,I}$ directly. In all our calculations we employ equation (14), where we take all mass components fully into account, without any further simplifications. For many combinations of model parameters, a round halo is too dense to explain the observed flaring (cf. Fig. 2). Albeit not entirely correct, we will determine the halo's contribution to the potential using equation (13) in those cases.

4 THE EFFECTS OF A LARGER GASEOUS VELOCITY DISPERSION

Equations (9)–(15) show that $q_{\rm H\,I}$ is a function of $\sigma_{\rm g}$, Θ_0 and R_0. On the other hand, the halo flattening inferred from the local stellar kinematics is a function of the Galactic constants and Σ_*. In a self-consistent model, $q_{1.1} \equiv q_{\rm H\,I}$, so that strong interrelations are imposed among the currently ill-determined values of R_0, Θ_0, Σ_* and $\sigma_{\rm g}$.

Below we investigate how the inferred halo flattening and stellar column density of a self-consistent model depend upon our choice of $\sigma_{\rm g}$. The value of $\sigma_{\rm g}$ can have significant effects on the inferred values of q and Σ_*. For example, in Paper I we assumed that the true velocity dispersion equals 9.2 km s^{-1}, and found an upper limit to the local rotation speed of about 190 km s^{-1}. Further, models with the IAU-recommended Galactic constants have prolate dark haloes ($q \sim 1.9$) and require a rather high local stellar column density of $\sim$55 M$_\odot$ pc^{-2}. Increasing $\sigma_{\rm g}$ would bring q and Σ_* down to more acceptable levels, and it might thus be worthwhile to treat $\sigma_{\rm g}$ as a free rather than as a fixed parameter.

However, observations of external galaxies imply that the velocity dispersion *declines* slightly in the radial range over which the Milky Way's flaring has been measured, by a factor of 1.12 ± 0.12 (Shostak & van der Kruit 1984; Dickey, Hanson & Helou 1990; Kamphuis 1993; Côté 1995; Olling 1996b; Sicking 1997). Furthermore, there is some evidence that $\sigma_{\rm g}$ in the outer Galaxy equals the value inside the solar circle (Blitz & Spergel 1991). Also, one would expect that a change in gaseous velocity dispersion would be reflected in a change of the residual motions of young stars with respect to the mean streaming field. Such changes have not been observed, neither in B stars nor in Cepheids (Brand & Blitz 1993; Pont et al. 1997). Thus an increase in gaseous velocity dispersion beyond the solar circle is not likely.

4.1 Non-thermal pressure terms

In Paper I we argued that the ISM beyond the optical disc comprises a single, isothermal component (the warm neutral medium). We now investigate the possibility that non-thermal pressures have to be included in the hydrostatic balance.

It is estimated that in the solar neighbourhood thermal motions, cosmic rays and magnetic fields contribute about equally to the interstellar pressure (Spitzer 1978; Kulkarni & Heiles 1988). However, note that the gas-layer width depends on the pressure *gradient*, not just the pressure. Incorporating the non-thermal pressure terms, the equation of hydrostatic equilibrium can be written as

$$\rho_{\rm g}(z)K_z(z) = \frac{{\rm d}P_{\rm G}}{{\rm d}z} + \frac{{\rm d}P_{\rm B}}{{\rm d}z} + \frac{{\rm d}P_{\rm C}}{{\rm d}z} = \frac{{\rm d}P_{\rm tot}}{{\rm d}z} \quad (18)$$

with $P_{\rm G} = \sigma_{\rm g}^2\rho_{\rm g}(z)$ the thermal gas pressure, $P_{\rm B} = B^2/8\pi$ the magnetic field pressure, and $P_{\rm C} = 1/3U_{\rm C}$ is the pressure due to cosmic rays with energy density $U_{\rm C}$. Taking the scale-heights of the kinetic, magnetic and cosmic ray energy density to be $z_{\rm G}$, $z_{\rm B}$ and $z_{\rm C}$, we write the pressure gradients as $\frac{{\rm d}P_{\rm G}}{{\rm d}z} = \frac{P_{\rm G}}{z_{\rm G}}$, $\frac{{\rm d}P_{\rm B}}{{\rm d}z} = \frac{P_{\rm B}}{z_{\rm B}}$ and $\frac{{\rm d}P_{\rm C}}{{\rm d}z} = \frac{P_{\rm C}}{z_{\rm C}}$.

4.2 Gas-layer support at R_0

In the solar circle neighbourhood the scale-heights $z_{\rm B}$ and $z_{\rm C}$ are $\kappa_{\rm B}$ and $\kappa_{\rm C}$ times larger than the gaseous scale-height [$\kappa_{\rm B} \sim 10$, $\kappa_{\rm C} \sim 4$; (e.g. Kulkarni & Heiles 1988; Rupen 1991)]. Following Spitzer (1978), we assume that the non-thermal pressure terms are proportional to the kinetic pressure: $P_{\rm B} = \alpha_{\rm B}P_{\rm G}$ and $P_{\rm C} = \alpha_{\rm C}P_{\rm G}$, with $\alpha_{\rm B} \sim 0.25$ and $\alpha_{\rm C} \sim 0.4$ in the solar circle neighbourhood. Using these parametrizations we find:

$$\rho_{\rm g}(z)K_z(z) \approx \sigma_{\rm g}^2\left(1 + \frac{\alpha_{\rm B}}{\kappa_{\rm B}} + \frac{\alpha_{\rm C}}{\kappa_{\rm C}}\right)\frac{{\rm d}\rho_{\rm G}}{{\rm d}z} \quad (19)$$

$$\approx (\sigma_{\rm g}')^2\frac{{\rm d}\rho_{\rm G}}{{\rm d}z}, \quad (20)$$

where we have lumped all terms contributing to the hydrostatic balance into a single unknown, the effective velocity dispersion $\sigma'_{\rm g}$. With the above simplifications and equations (10) and (16), it becomes possible to estimate the effects of non-thermal pressure support on the thickness of the gas layer and the inferred shape of the dark matter halo:

$$\left.\frac{\rm FWHM_{GBC}}{\rm FWHM_G}\right|_{R_0} \approx \frac{\sigma'_{\rm g}}{\sigma_{\rm g}} = \sqrt{1+\frac{\alpha_{\rm B}}{\kappa_{\rm B}}+\frac{\alpha_{\rm C}}{\kappa_{\rm C}}} \sim 1.06 \tag{21}$$

$$\left.\frac{q_{\rm GBC}}{q_{\rm G}}\right|_{R_0} \approx \left(\frac{\sigma_{\rm g}}{\sigma'_{\rm g}}\right)^2 \sim 0.89, \tag{22}$$

where the subscripts GBC indicates that the gaseous, magnetic and cosmic ray terms are taken into account in the hydrostatic balance of the gas layer. Thus, neglecting the non-thermal contribution to the pressure balance in the local ISM leads to a gas layer width that is underestimated by a few per cent only. Similarly, a slightly more flattened halo is required if non-thermal pressure support were important in the solar circle neighbourhood.

4.2.1 *Non-thermal support, or not?*

The above statements are at odds with the current paradigm (cf. Binney & Merrifield 1998, problem 9.7), which states that there exists significant non-thermal pressure support of the gas layer in the solar circle neighbourhood. The argument in support of this paradigm is that models without non-thermal pressure support underpredict the observed gas-layer widths. However, the model predictions depend sensitively on the values of the Galactic constants. Our models with small values for R_0 and Θ_0 show only a small discrepancy between the model and observed widths, while a large width difference exists for models with IAU-standard Galactic constants (Paper I, fig. 5). Furthermore, the gas-layer width depends sensitively on the local stellar column density as well as the functional form of the vertical density distribution. For example, the gas layer is almost 40 per cent thinner in the case where the stellar vertical density distribution is exponential rather than sech^2 (van der Kruit 1988).

In fact, if the potential in the solar circle neighbourhood were fully determined by the stellar disc, and the H I were truly isothermal, then the predicted width via equation (12) *overpredicts* the observed width (cf. Table 1). The other contributors to the potential decrease the model width slightly (cf. equation 14), in better agreement with the observed width. We conclude that the paradigm of significant non-thermal pressure support in the solar circle neighbourhood is inaccurate, and that the observed H I width at the solar circle is consistent with 'thermal' pressure support only (cf. equation 21).

4.3 Gas-layer support at $2R_0$

Since we only employ the H I thickness measurements at large radii as a constraint in our mass models, let us try to guess the value of $\sigma'_{\rm g}$ at $\sim 2R_0$.

The gas density in the outer Galaxy is about 4 times smaller than at R_0 as a result of the decrease in column density (factor of 2) and the increase in thickness (factor of 2). To make a conservative estimate as to the importance of the non-thermal terms at large distances, we assume that the magnetic field strength, the cosmic ray energy density and their vertical gradients equal the values in the solar neighbourhood. Furthermore, we assume that $\sigma_{\rm g}$ remains unchanged. With these assumptions, the α values at $2R_0$ are 4 times larger than at $R = R_0$, while the κ values are decreased by a factor of 2. Thus the effective velocity dispersion and the inferred halo shape are strongly affected:

$$\left.\frac{\sigma'_{\rm g}}{\sigma_{\rm g}}\right|_{2R_0} = \sqrt{1+\frac{4\alpha_{\rm B}(R_0)}{\kappa_{\rm B}(R_0)/2}+\frac{4\alpha_{\rm C}(R_0)}{\kappa_{\rm C}(R_0)/2}} \sim \sqrt{2} \tag{23}$$

$$\left.\frac{q_{\rm GBC}}{q_{\rm G}}\right|_{2R_0} \approx \left(\frac{\sigma_{\rm g}}{\sigma'_{\rm g}}\right)^2 \sim 0.5. \tag{24}$$

On the basis of this overestimation, it appears that the gas layer is significantly out of thermal equilibrium at large radii. Do we expect this to be the case? Two effects reduce the importance of the non-thermal contribution. First, because the B-field is probably (co-spatial) 'frozen in' with the ionized part of the ISM, its scale-height is probably twice as large at $2R_0$ as at R_0 (just like the H I). Thus the solar neighbourhood value for $\kappa_{\rm B}(2R_0)$ should be used in equation (23). Second, radio-continuum measurements of external galaxies suggest that high cosmic ray fluxes are closely associated with the sites of star formation (Bicay & Helou 1990). Since active star formation ceases to exist beyond $\sim 1.5R_0$, the $\alpha_{\rm C}$-term in equation (23) vanishes. Thus, in a more realistic treatment of the non-thermal pressure terms, their effect on the vertical equilibrium of gas at large radii is much reduced:

$$\left.\frac{\sigma'_{\rm g}}{\sigma_{\rm g}}\right|_{2R_0} = \sqrt{1+\frac{4\alpha_{\rm B}(R_0)}{\kappa_{\rm B}(R_0)}} = \sqrt{1.1} \sim 1.05 \tag{25}$$

$$\left.\frac{q_{\rm GBC}}{q_{\rm G}}\right|_{2R_0} \approx \left(\frac{\sigma_{\rm g}}{\sigma'_{\rm g}}\right)^2 \sim 0.9. \tag{26}$$

Further, if the magnetic field strength decreases with Galactocentric radius, the above estimates should be even closer to unity. Thus, realistic estimates of the importance of non-thermal pressure terms in the equation of hydrostatic equilibrium indicate that the thickness of the H I layer is not much affected, neither in the inner, nor in the outer Galaxy.

Finally, it is worth mentioning that there is both theoretical and empirical evidence that non-thermal pressure support is small even when simplified calculations indicate that they may dominate $\mathrm{d}P_{\rm g}/\mathrm{d}z$. From a theoretical perspective one finds that the vertical balance is affected only if the magnetic field is horizontally stratified, a configuration that is unstable (Parker 1966), and which is thus not expected to exist on a global scale in the Milky Way. In fact, 3D simulations of the growth of the Parker instability show that the gas is almost entirely supported by thermal pressure within the first four scale-heights (Kim et al. 1998). On the observational side, Rupen (1991) presents evidence that the non-thermal pressure gradients equal 400 per cent of the thermal pressure gradient in NGC 891, and 50 per cent in NGC 4565. Since the luminous mass distributions in these galaxies are very similar, one would expect very different gas layer widths if non-thermal effects were indeed important. In fact, these two galaxies have almost indistinguishable flaring curves, and we can conclude that thermal pressure gradients dominate (Rupen 1991; Olling 1996a).

To summarize, simplified theoretical considerations indicate that non-thermal pressure support could dominate the hydrostatic balance if extreme assumptions about the magnetic field geometry and the cosmic ray energy density are made. More realistic assumptions regarding the vertical gradients of $P_{\rm B}$ and $P_{\rm C}$, as well as observational data, lead to the opposite conclusion.

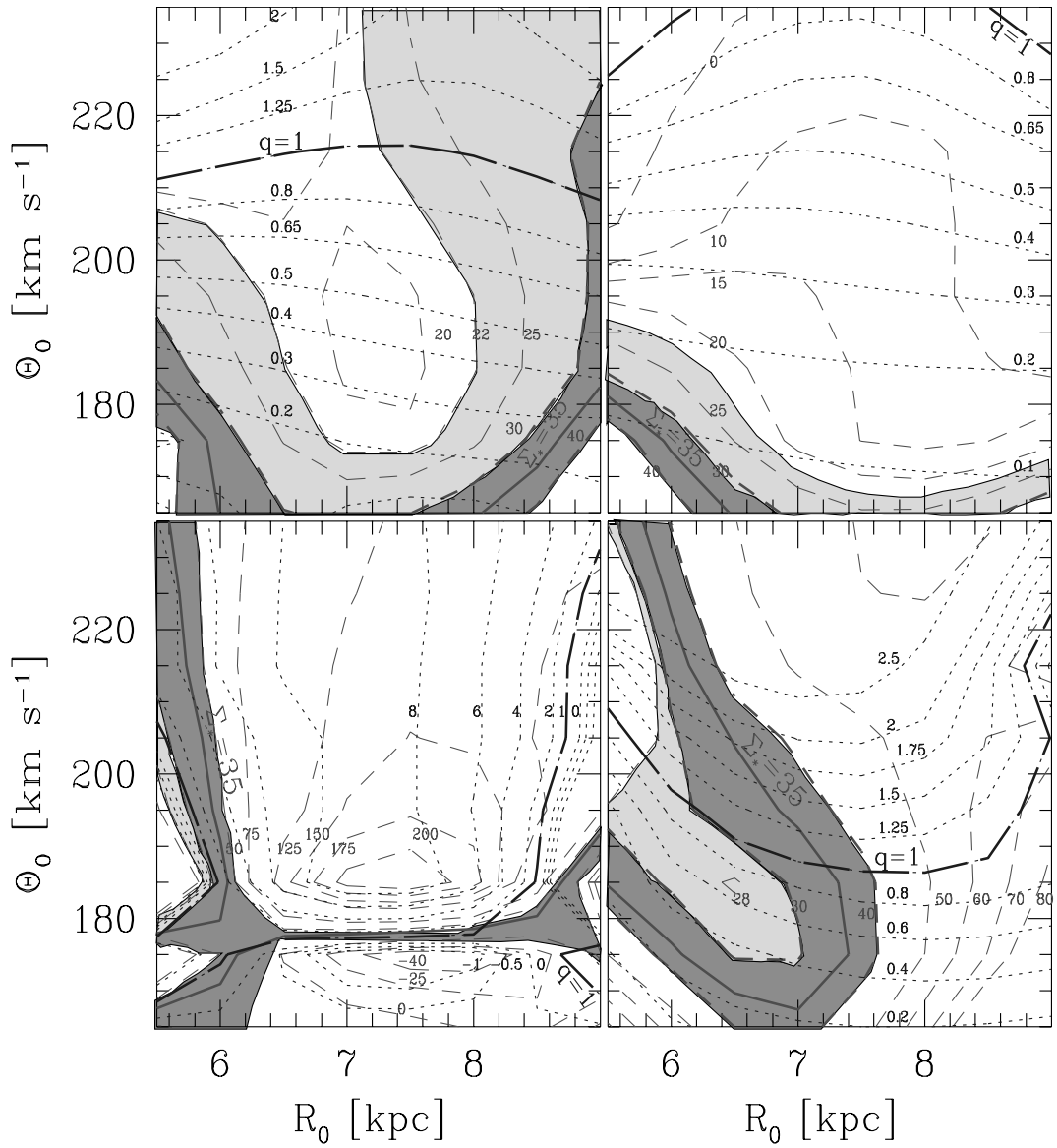

Figure 2. Here we present the *mutually consistent* set of Galactic constants, stellar column density in the solar circle neighbourhood (Σ_*; long-dashed lines) and halo flattening (q; dotted lines). The individual panels show the results of the calculation for several values of σ_g'/σ_g : 0.85 ($\sigma_g' = 8\,\mathrm{km\,s^{-1}}$, lower left), 1.0 ($\sigma_g' = 9.2\,\mathrm{km\,s^{-1}}$, lower right), 1.15 ($\sigma_g' = 10.5\,\mathrm{km\,s^{-1}}$, upper left), and 1.30 ($\sigma_g' = 12\,\mathrm{km\,s^{-1}}$, upper right). The oblate–prolate boundary is indicated by the heavy dot-dashed line. The heavy full line and the heavy dashed line correspond to KG89b's determination of Σ_*, and the $\pm 1\sigma$ values. The upper limit of GBF97's determination of the stellar column density corresponds to the $\Sigma_* \sim 30\,\mathrm{M_\odot\,pc^{-2}}$ contour. Both the halo flattening and stellar column are determined to ~ 6 per cent accuracy (see also Appendix C). Because the Galactic constants, Σ_*, and q, have to be mutually consistent, one cannot arbitrarily choose the four parameters. Fixing one of the four parameters severely restricts the other three. Any two parameters follow immediately from any choice of the other two, for a given σ_g. In the shaded region of parameter space, the mass of the stellar disc is as measured by KG89b (dark shading) and GBF97 (light shading).

In the next paragraph we will investigate the effects of significant non-thermal pressure support by treating the gaseous velocity as an unknown, notwithstanding the indications that non-thermal pressure support is actually small in the outer Galaxy. Based on the arguments presented above, we expect σ_g' to lie between $\sim$0.85 and $\sqrt{2}$ times the default value of $9.2\,\mathrm{km\,s^{-1}}$, while a more realistic upper limit to σ_g'/σ_g might be 1.05 (cf. equation 25).

4.4 Constraints on the pressure term

In this section we address the question as to how the interrelations between the Galactic constants, Σ_* and q, are affected when assuming that σ_g is unknown. We follow the procedure to determine the halo flattening as outlined in the Introduction (and Paper I) for several trial values of σ_g ($\sigma_g' = 8.0$, 8.6, 9.2, 9.9, 10.5, 12 and $14\,\mathrm{km\,s^{-1}}$), and on the same $R_0 - \Theta_0$ grid as in Paper I. As predicted by equation (17), the inferred halo flattening and stellar column density are rather sensitive to the adopted value of σ_g'. In Fig. 2 we present q (dotted lines) and Σ_* (long-dashed-lines) as calculated for increasing values of σ_g', from left to right, and from top to bottom. The oblate region of parameter space, below the heavy dot-dashed line, is strongly restricted if $\sigma_g'/\sigma_g < 1$ (lower-left panel), while essentially the whole range of the Galactic constants is allowed if the effective dispersion is as large as $12\,\mathrm{km\,s^{-1}}$ (upper-right panel). From these figures we can also infer

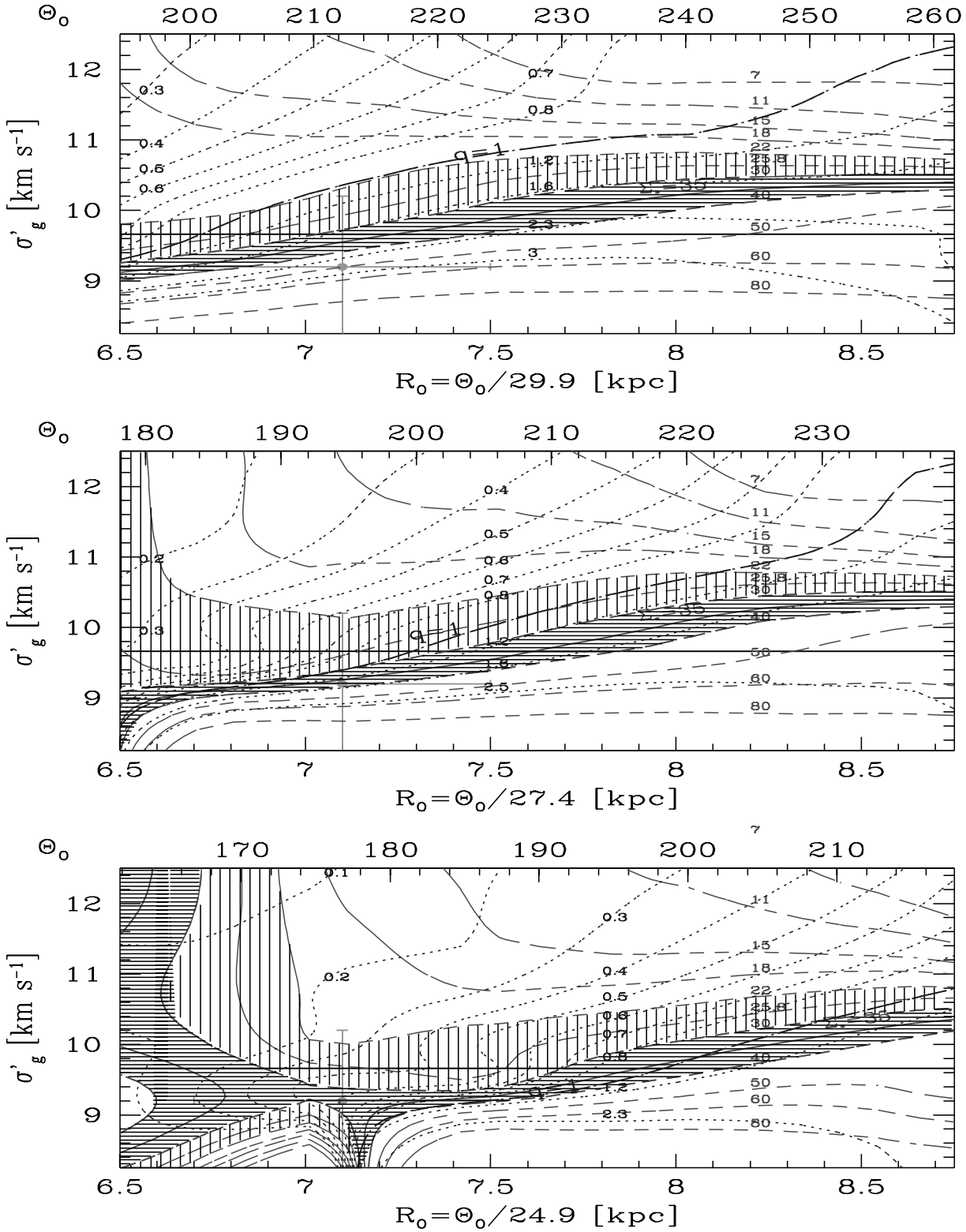

Figure 3. In this figure we present the interrelations between the adopted value of the gaseous velocity dispersion (σ'_g) and the Galactic constants. The line coding is the same as in Fig. 2. This figure was generated by extracting the halo flattening and Σ_* values along the lines $\Theta_0/R_0 = 24.9, 27.4$ and 29.9 (from top to bottom), for several values of the effective gaseous velocity dispersion. The fat cross represents our best estimate for the Galactic constants ($R_0 = 7.1 \pm 0.4$ kpc, $\Theta_0 = 184 \pm 8$ km s^{-1}; Olling & Merrifield 1998c), and the gaseous velocity dispersion ($\sigma_g = 9.2 \pm 1$ km s^{-1}; Malhotra 1995). The thick horizontal line represents our theoretical expectation as to the maximum value of σ'_g (equation 25). Large effective velocity dispersions require flattened haloes so that the model gas layer widths are as thin as observed. Round, and even prolate, haloes are found for small σ'_g values. In the shaded region of parameter space, the mass of the stellar disc is as measured by KG89b (horizontal dark shading) and GBF97 (vertical light shading).

that the mass of the stellar disc, if measured accurately, constrains the allowed range of σ_g'.

Values for σ_g' that are as much as 30 per cent larger than the default value (upper-right panel of Fig. 2) are completely excluded because of the very small stellar disc masses required. On the other hand, lower velocity dispersions need lower density (rounder) haloes, and hence a more massive stellar disc, for given Galactic constants. This is indeed what is observed in the lower-left panel of Fig. 2 for $\Theta_0 \gtrsim 175\,\mathrm{km\,s^{-1}}$. However, below $\Theta_0 \sim 175\,\mathrm{km\,s^{-1}}$, the situation is much more chaotic (extreme negative values for Σ_* and q), which is the result of the fact that the H I flaring and the stellar kinematical constraints are mutually exclusive (Appendix B). In fact, an effective velocity dispersion $\lesssim 8\,\mathrm{km\,s^{-1}}$ is essentially ruled out.

4.5 Other constraints

In order to take all constraints properly into account, we should present a three-dimensional plot with R_0, Θ_0 and σ_g' as the axes. Because this is a little tedious, we opt to determine the halo flattening and Σ_* along lines of constant Ω_0. We select Ω_0 values which bracket the uncertainty of the proper motion of SgrA* (Reid et al. 1999). In each of the three panels of Fig. 3 ($\Omega_0 = 29.9, 27.4$ and $24.9\,\mathrm{km\,s^{-1}\,kpc^{-1}}$, from top to bottom) we present contours of constant halo flattening by dotted lines as a function of R_0 and σ_g'. The heavy dot-dashed line is the round-halo contour. The hashed parts of the diagram depict regions of parameter space where $\Sigma_* = 35 \pm 5\,\mathrm{M_\odot\,pc^{-2}}$ (heavy horizontal hash) and $\Sigma_* = 27.8 \pm 3.8\,\mathrm{M_\odot\,pc^{-2}}$ (light vertical hash). These column density ranges correspond to the stellar disc mass as determined by KG89b and GBF97, respectively. In Fig. 3 we also plot our estimate to the upper limit of the non-thermal pressure support ($\sigma_g' \sim 1.05\sigma_g$) as the thick horizontal line. The cross at $(R_0, \sigma_g') = (7.2, 9.2)$ corresponds to the value of R_0 derived from the Oort constant (Olling & Merrifield 1998c) and the standard value of the gaseous velocity dispersion.

A general feature of these diagrams is that flatter haloes are found in regions with large values of σ_g'. This arises naturally from the fact that a stronger gravitational pull is needed to constrain a gas layer with additional pressure support, for a given observed thickness (see also equation 13). These figures also clearly show that regions with large DM densities, due to either large Θ_0 or small q, have low stellar column density in the solar neighbourhood. We can seen that significant non-thermal pressure support, which we define here as having $\sigma_g' = \sqrt{2}\sigma_g \sim 13\,\mathrm{km\,s^{-1}}$, requires very highly flattened DM haloes *and* very small stellar columndensities in the solar neighbourhood. Such strong non-thermal pressure support is thus ruled out.

Several other generic conclusions can be drawn from Fig. 3. First, highly flattened haloes are possible for realistic values of Σ_* only if $R_0 \lesssim 7\,\mathrm{kpc}$, and only for small values of Ω_0. Second, large values for R_0, an acceptable stellar column density, and an oblate halo occur only if the angular velocity of the Milky Way is small, whatever the value of the effective velocity dispersion. Third, the extra degree of freedom associated with σ_g' does not greatly influence the inferred halo flattening if a good constraint on Σ_* can be used. Finally, the combined constraints set by the observed stellar column density and the halo's oblateness severely restrict the allowed range for σ_g', in particular for $R_0 \gtrsim 7\,\mathrm{kpc}$.

More specific results follow if we are willing to make more restrictive assumptions. For example, if we assume that $R_0 \gtrsim 7$ and $\sigma_g' \leq 10.2$, we find $q \gtrsim 1.0 (\Omega_0 = 29.9)$, $q \gtrsim 0.65 (\Omega_0 = 27.4)$, and $q \gtrsim 0.2 (\Omega_0 = 24.9)$. In the case where $R_0 \gtrsim 8\,\mathrm{kpc}$, $q \gtrsim 2$, $q \gtrsim 1.3$ and $q \gtrsim 0.8$ for the same angular velocities. Alternatively, when choosing particular values for the Galactic constants, simple relations between the remaining three parameters of the mass model follow. For example, taking the IAU-recommended values for R_0 and Θ_0 ($8.5\,\mathrm{kpc}$ and $220\,\mathrm{km\,s^{-1}}$) we find $q \sim 2.26 - 0.90 \times \mathrm{d}\sigma_g' + 0.11 \times (\mathrm{d}\sigma_g')^2$ *and* $\Sigma_* \sim 65.6 - 35.2 \times \mathrm{d}\sigma_g' + 4.8 \times (\mathrm{d}\sigma_g')^2$, with $\mathrm{d}\sigma_g' = \sigma_g' - 9.2$. Also, with the standard value for the gaseous velocity dispersion we find: $\Theta_0 (q \leq 1) \lesssim 187 + 5 \times \mathrm{d}R_0^2$ *and* $\Sigma_* (0.5 \lesssim q \lesssim 1) \sim 37.5 + 18.4 \times \mathrm{d}R_0 + 8.5 \times \mathrm{d}R_0^2$, with $\mathrm{d}R_0 = R_0 - 7.5$ (cf. Fig. 2, the lower-right panel).

An inspection of the lower two panels of Fig. 3 reveals that rather tight constraints can be placed on the halo shape, the local angular velocity and the effective velocity dispersion if the halo is oblate and $30 \lesssim \Sigma_* \lesssim 40\,\mathrm{M_\odot\,pc^{-2}}$ and $R_0 \gtrsim 7\,\mathrm{kpc}$. In that case we find: $24.9 \lesssim \Omega_0 \lesssim 27.4\,\mathrm{km\,s^{-1}\,kpc^{-1}}$, $0.5 \lesssim q \leq 1$, and $8.6 \lesssim \sigma_g' \lesssim 10.3\,\mathrm{km\,s^{-1}}$. If we impose the additional constraint that the non-thermal pressure support is limited to 5 per cent as derived in equation (25), it follows that the Sun's distance to the Galactic Centre is less than 8 kpc, and that the rotation speed of the Milky Way is less than $200\,\mathrm{km\,s^{-1}}$ at the solar circle.

The stellar disc mass provides a strong constraint on the effective velocity dispersion of the gas: a low disc mass requires more dark matter, which would lead to a thinner gas layer in the outer Galaxy if σ_g' were not increased. For example, if the stellar disc mass exceeds $22\,\mathrm{M_\odot\,pc^{-2}}$, Fig. 3 shows that the effective velocity dispersion has an upper bound of about $10.5\,\mathrm{km\,s^{-1}}$, so that the non-thermal pressure support can not exceed 14 per cent.

5 SUMMARY AND CONCLUSIONS

In Paper I we showed that the constraints on the dark matter density in the solar neighbourhood and the outer Galaxy place tight limits on the choice of the Galactic constants, the mass of the stellar disc, and the dark halo's flattening. The internal errors for this procedure are of order 6 per cent for both the halo flattening and the local stellar column density (see Appendix C).

In this paper we present the analytical tools that allow for an efficient search through parameter space. Employing these tools, we extend the analysis of Paper I by investigating the effects of the ill-determined contribution of non-thermal pressure support on the H I flaring, and the consequences for the inferred R_0, Θ_0, Σ_* and q values. The strongest constraints available are the observed Θ_0/R_0 ratio, the mass of the stellar disc, and the fact that the dark halo is almost certainly oblate. Taken together, these constraints rule out substantial contributions to the support of the H I layer by cosmic ray pressure or magnetic fields if the Sun's distance to the Galactic Centre is $\geq 7\,\mathrm{kpc}$, in agreement with theoretical predictions. We find that the Milky Way's dark matter halo is close to spherical for all but the smallest values of R_0 or Θ_0. A dark matter halo as flattened as $q = 0.2$ is possible only if our distance to the Galactic Centre is smaller than about 6.8 kpc.

It is possible to construct a self-consistent oblate model of the Galaxy with $R_0 = 8.5\,\mathrm{kpc}$ and $\Theta_0 = 220\,\mathrm{km\,s^{-1}}$, but only if the local stellar column density is less than about $18\,\mathrm{M_\odot\,pc^{-2}}$, *and* $\sigma_g' \gtrsim 11\,\mathrm{km\,s^{-1}}$.

KG91's determination of the column density of matter within 1.1 kpc of the plane ($71 \pm 6\,\mathrm{M_\odot\,pc^{-2}}$) is robust and valid over a wide range of Galactic constants and disc scalelengths. For the stellar contribution to this total mass we suggest a *consensus* average of $\Sigma_* = 35$ and a *consensus* error of $10\,\mathrm{M_\odot\,pc^{-2}}$.

If $R_0 \gtrsim 7\,\mathrm{kpc}$, then the dark halo of the Milky Way is fairly close to spherical, independent of the amount of non-thermal pressure support. Such a round halo argues against dissipational baryons as

a viable dark matter candidate. Further, since all other baryonic dark matter candidates have already been observationally excluded (Hegyi & Olive 1986), we must conclude that the dark matter halo of the Milky Way is probably made up of something altogether more exotic (MACHOs, neutrinos, axions, neutralinos …). Even in the solar circle neighbourhood, there are non-negligible quantities of this material: our proposed dark halo models imply that it amounts to some $0.42\,\mathrm{GeV}/c^2$ per cubic centimetre or $(11 \pm 5)\,\mathrm{m\,M_\odot\,pc^{-3}}$. The direct detection of this material remains a challenge for experimental physicists.

Employing the local disc mass and the flaring of the Galactic H I layer, we find strong correlations between the parameters of axisymmetric mass models. We presented several examples in the previous section. Since we make strong predictions as to the values of R_0, Θ_0, Σ_*, q and $\sigma'_{\rm g}$ (Figs 2 and 3), our models can be subjected to experimental verification. For example, all parameters but $\sigma'_{\rm g}$ could be determined using astrometric data from future astrometric space missions such as *FAME*, *SIM* and *GAIA*. Such high-precision data are ideally suited to support, or falsify, the models we propose here. It would also be worthwhile to investigate the effects of deviations from axisymmetry on the inferred halo shape and rotation speed. Whatever the outcome, we will learn a great deal more about the structure and dynamics of the Milky Way galaxy.

ACKNOWLEDGMENTS

We thank Andy Newsam, Irini Sakelliou, Konrad Kuijken, Marc Kamionkowski, Jacqueline van Gorkom, Chris McKee and James Binney for useful discussions. We also thank the referee for valuable suggestions for improvements. Much of this research was performed by the authors while at the University of Southampton and while RPO was at Rutgers University. RPO thanks Columbia University's Astronomy department for its hospitality. This research has made use of NASA's Astrophysics Data System Abstract Service.

REFERENCES

Bahcall J. N., 1984a, ApJ, 276, 156
Bahcall J. N., 1984b, ApJ, 276, 169
Bahcall J. N., Flynn C., Gould A., 1992, ApJ, 389, 234
Begeman K., 1987, PhD thesis, Groningen Univ.
Begeman K., 1989, A&A, 223, 47
Bergstrom L., Ullio P., Buckley J. H., 1998, Astroparticle Phys., 9, 137
Bicay M. D., Helou G., 1990, ApJ, 362, 59
Bienaymé O., Robin A. C., Crézé M., 1987, A&A, 180, 94
Binney J., Merrifield M., 1998, Galactic Astronomy. Princeton Univ. Press, Princeton, NJ 08540
Blitz L., Spergel D. N., 1991, ApJ, 370, 205
Bosma A., 1981, AJ, 86, 1825
Bottema R., 1993, A&A, 275, 16
Brand J., Blitz L., 1993, A&A, 275, 67
Braun R., 1997, ApJ, 484, 637
Broeils A., 1992, PhD thesis, Groningen Univ.
Bronfman L., Cohen R. S., Alvarez H., May J., Thaddeus P., 1988, ApJ, 324, 248
Burton W. B., 1988, in Verschuur G. L., Kellermann K. I., eds, Galactic and Extragalactic Radio Astronomy. Springer, Berlin, p. 295
Casertano S., van Gorkom J. H., 1991, AJ, 101, 1231
Côté S., 1995, PhD thesis, Mt. Stromlo and Siding Spring Observatories, Australian National University
Crézé M., Chereul E., Bienaymé O., Pichon C., 1998, A&A, 329, 920
Crézé M., Robin A. C., Bienaymé O., 1989, A&A, 211, 1
Dehnen W., Binney J., 1998, MNRAS, 294, 429
Dickey J. M., Hanson M. M., Helou G., 1990, ApJ, 352, 522
Flynn C., Fuchs B., 1994, MNRAS, 270, 471
Freudenreich H. T., 1996, ApJ, 468, 663
Freudenreich H. T., 1998, ApJ, 492, 495
Gates E. I., Gyuk G., Turner M. S., 1995, Phys. Rev. Lett., 74, 3724
Gould A., Bahcall J. N., Flynn C., 1997, ApJ, 482, 913 (GBF97)
Hegyi D., Olive K. A., 1986, ApJ, 303, 56
Kamphuis J., 1993, PhD thesis, Groningen Univ.
Kent S. M., 1987, AJ, 93, 816
Kent S. M., 1992, ApJ, 387, 181
Kent S. M., Dame T. M., Fazio G., 1991, ApJ, 378, 131
Kerr F. J., Lynden-Bell D., 1986, MNRAS, 221, 1023
Kim J., Hong S. S., Ryu D., Jones T. W., 1998, ApJ, 506, L139
Kuijken K., Gilmore G., 1989a, MNRAS, 239, 571 (KG89a)
Kuijken K., Gilmore G., 1989b, MNRAS 239, 605 (KG89b)
Kuijken K., Gilmore G., 1991, ApJ, 367, L9 (KG91)
Kulkarni S. R., Heiles C., 1988, in Hollenbach D. J., Thronson H. A., Jr., eds, Interstellar Processes. Astrophysics and Space Science Library, Vol. 134. Reidel, Dordrecht, p. 87
Lake G., Feinswog L., 1989, AJ, 98, 166
Malhotra S., 1995, ApJ, 448, 138
McGaugh S. S., de Blok W. J. G., 1998, ApJ, 499, 66
Merrifield M. R., 1992, AJ, 103, 1552
Navarro J., Frenk C. S., White S. D. M., 1996, ApJ, 462, 563
Olive K. A., Steigman G., 1995, ApJS, 97, 490
Olling R. P., Merrifield M. R., 1998a, in Zaritsky D., ed., ASP Conf. Ser. Vol. 136, Galactic Haloes. Astron. Soc. Pac., San Francisco, p. 219 (astro-ph/9711157)
Olling R. P., Merrifield M. R., 1998b, in Zaritsky D., ed., ASP Conf. Ser. Vol. 136, Galactic Haloes. Astron. Soc. Pac., San Francisco, p. 216 (astro-ph/9710224)
Olling R. P., Merrifield M. R., 1998c, MNRAS, 297, 943
Olling R. P., Merrifield M. R., 2000, MNRAS, 311, 361 (Paper I)
Olling R. P., 1995, AJ, 110, 591
Olling R. P., 1996a, AJ, 112, 481
Olling R. P., 1996b, AJ, 112, 457
Parker E. N., 1966, ApJ, 145, 811
Persic M., Salucci P., Stel F., 1996, MNRAS, 281, 27
Pont F., Queloz D., Bratchi P., Mayor M., 1997, A&A, 318, 416
Reid M. J., 1993, ARA&A, 31, 345
Reid N., Majewski S. R., 1993, ApJ, 409, 635
Robin A. C., Crézé M., Mohan V., 1992, ApJ, 400, L25
Rubin V. C., Ford W. K., Thonnard N., 1980, ApJ, 238, 471
Rupen M. P., 1991, PhD thesis, Princeton Univ.
Sackett P. D., 1997, ApJ, 483, 103
Sackett P. D., Sparke L. S., 1990, ApJ, 361, 408
Shostak G. S., van der Kruit P. C., 1984, A&A, 132, 20
Sicking F., 1997, PhD thesis, Groningen Univ.
Spitzer L., 1978, Physical Processes in the Interstellar Medium. John Wiley & Sons, New York
van Albada T. S., Sancisi R., 1986, Phil. Trans. R. Soc. Lond. A, 320, 447
van der Kruit P. C., 1988, A&A, 192, 117
Wielen R., 1974, Highlights of Astronomy, 3, 395
Wouterloot J. G. A., Brand J., Burton W. B., Kwee K. K., 1990, A&A, 230, 21

APPENDIX A: MORE ON THE VERTICAL DISC–HALO CONSPIRACY

In Section 3.1 we reviewed the stellar kinematical route to determine the local stellar column density. In this appendix we try to emulate and check this method in some detail. In order to do so, we calculate the exact vertical force law $K_{z,\rm exact}$ for a limited number of Galaxy models listed in Table 2 using the global approach (Section 3.3; cf. Olling 1995). We also compute an

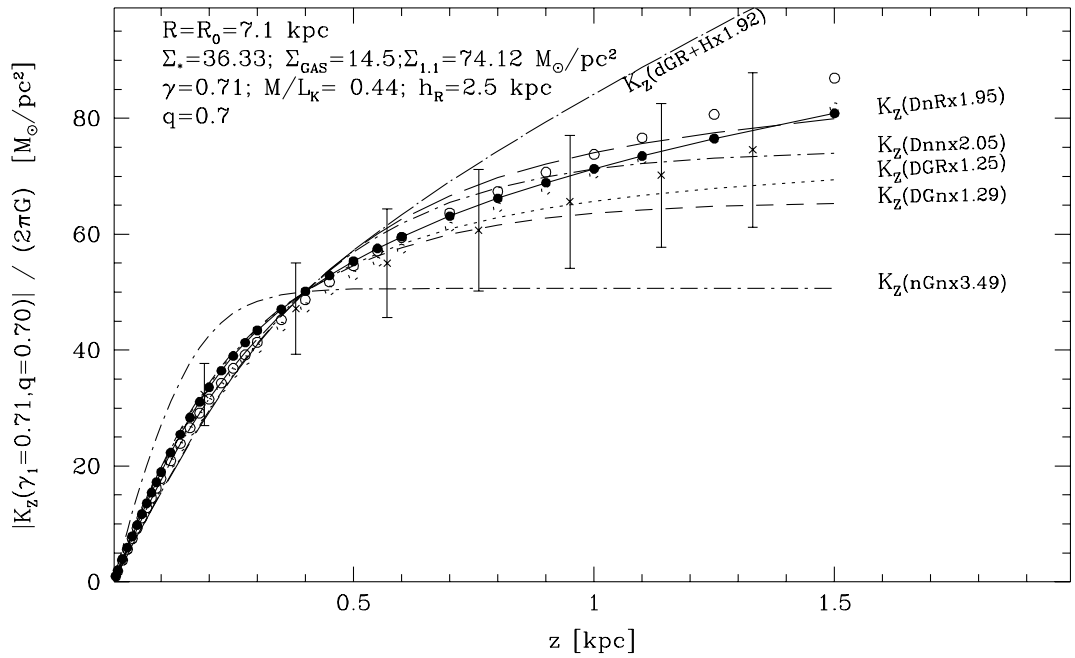

Figure A1. We present the exact vertical force (filled circles) at Galactocentric distance R_0 for a model that almost reproduces the values for Σ_* and $\Sigma_{\rm tot}^{1.1}$ proposed by KG89b and KG91. The local approximation to the exact force law that uses the slope of the rotation curve (open circles) or assumes a flat rotation curve (dashed open circles) is also indicated. Some other models in which the DM is distributed like various superpositions of the known components are also plotted: (1) $\rho_{\rm DM} = 1.29 \times (\rho_* + \rho_{\rm g})$ (labelled 'DGnx1.29'); (2) $\rho_{\rm DM} = 1.25 \times (\rho_* + \rho_{\rm g} + \rho_{\rm rot})$ ('DGRx1.25'); (3) $\rho_{\rm DM} = 2.05 \times \rho_*$ ('Dnnx2.05'); (4) $\rho_{\rm DM} = 1.95 \times (\rho_* + \rho_{\rm rot})$ ('DnRx1.95'); (5) $\rho_{\rm DM} = 3.49 \times \rho_{\rm g}$ ('nGnx3.49'). For the curve labelled 'dGR+Hx1.92' we used a smaller column density of stars 25.8 $M_\odot\,pc^{-2}$ (Gould, Bahcall & Flynn 1997), and multiplied the halo contribution by 1.92. Most of the models have very similar force laws in the region close to the plane (see also Table A1). We also include KG89b's vertical force law and the errors thereupon (crosses with error bars).

Table A1. The accuracy to which various erroneous density distributions can reproduce the true vertical force. The first four columns describe which $\rho(z)$ was used (cf. equation A2). The next three columns indicate the average ratio of $K_{z,\rm true}/K_{z,\rm err}$ over the vertical ranges indicated [0–0.4 kpc (Z1), 0.4–0.8 kpc (Z2), and 0.8–1.2 kpc (Z3)]. The typical variation within these radial ranges is a few per cent, except for the gas-only case where it can be up to 35 per cent. We also indicate the model values for Σ_* and $\Sigma_{\rm tot}^{1.1}$, in units of $M_\odot\,pc^{-2}$. The last two lines give the average and standard deviations of the lines above (excluding the gas-only model).

X_d	$X_{\rm g}$	$X_{\rm rot}$	$X_{\rm h}$	Z1	Z2	Z3	Σ_*	$\Sigma_{\rm tot}^{1.1}$
1.25	1.25	1.25	0.00	1.03	0.99	0.93	45.4	63.6
1.29	1.29	0.00	0.00	0.95	1.04	1.17	46.9	65.6
2.05	0.00	0.00	0.00	0.85	1.03	1.01	74.5	74.5
1.95	0.00	1.95	0.00	0.85	1.03	1.04	70.8	70.8
0.00	3.49	0.00	0.00	1.35	0.90	0.72	0.0	50.6
1.40	1.00	1.00	0.03	1.03	0.99	0.93	50.9	66.1
1.25	1.00	1.00	0.46	1.03	0.99	0.93	45.4	70.6
1.00	1.00	1.00	1.17	0.97	1.02	1.08	36.3	78.1
0.74	1.00	1.00	1.92	0.95	1.04	1.17	26.9	86.1
0.50	1.00	1.00	2.59	0.93	1.06	1.24	18.2	92.9
0.25	1.00	1.00	3.30	0.92	1.08	1.33	9.1	100.4
0.12	1.00	1.00	3.67	0.91	1.09	1.37	4.4	104.3
							39 ± 58%	77 ± 21%

approximation to $K_{z,\rm exact}$ from the local mass distribution (Section 3.3; cf. Olling 1995), which follows from an integration of the Poisson equation:

$$K_{z,\rm local}(z) = -4\pi G \int_0^z {\rm d}z' [\rho_{\rm m}(z') + \rho_{\rm rot}], \qquad \text{(A1)}$$

with $\rho_{\rm m}$ the matter density, $\rho_{\rm rot} (\equiv \frac{-2}{4\pi G} \frac{V_{\rm rot}}{R} \frac{{\rm d}V_{\rm rot}}{{\rm d}R})$ a pseudo-density which arises from gradients in the rotation curve, and K_z the vertical force per unit mass.

In Fig. A1 we present true vertical force (filled circles) and the local approximation (open circles) for one particular combination of parameters which lie close to the best estimates for the Milky Way (KG91; Olling & Merrifield 1998c). We see that in the solar circle neighbourhood and close to the plane, the local

approximation is reasonably accurate[10] and can be used as an approximation to the true vertical force law. Significant deviations from the true K_z only occur above approximately 800 pc. We also include the observationally determined K_z [crosses with error bars; KG89b's equation (1) with $D = 250$ pc].

Now we investigate the possibility that the actual DM density law differs from the distribution in our models (equation 1). Choosing a different DM distribution while keeping the observed K_z fixed requires a different luminous mass distribution. As a simple test case, we plot a model where the DM density is multiplied by 1.92 (labelled 'dGR + Hx1.92' in Fig. A1). In this case, we have to decrease the stellar column density to the GBF97 value ($25.8\,M_\odot\,pc^{-2}$) in order to keep K_z approximately unchanged. Next, we consider DM distributions inspired by Bahcall's 'P' models (1984b), where the DM density is assumed to be a linear combination of the known components:

$$\rho_{\rm err} = X_d \times \rho_d + X_{\rm g} \times \rho_{\rm g} + X_{\rm h} \times \rho_{\rm h} + X_{\rm rot} \times \rho_{\rm rot}, \qquad \text{(A2)}$$

where the subscripts d, g and h denote the disc, gas, and halo components, respectively. Using this formalism, we can calculate the columndensities of all components (ISM, stars, DM and $\Sigma_{\rm tot}^{1.1}$) which arise from a particular choice of the X_i-values. From such an erroneous density distributions ($\rho_{\rm err}$) we determine the erroneous vertical force ($K_{z,\rm err}$) using equation (A1). We present the $K_{z,\rm true}/K_{z,\rm err}$ ratio, averaged in several z-height ranges, in Table A1 (columns 5–7). In this table we also list the X_i, Σ_* and $\Sigma_{\rm tot}^{1.1}$ values for some models. In addition to the P-models, we also evaluate models in which we keep the ISM and $\rho_{\rm rot}$ contributions fixed while varying the stellar and DM densities such that the force at 400 pc above the plane equals the true value. From Table A1 we see that it is possible to decrease Σ_* by more than an order of magnitude and simultaneously increase $X_{\rm h}$ without altering $K_z(|z| \leq 800\,{\rm pc})$ substantially. It seems that the vertical distribution of dark and stellar matter conspire in such a way that their relative contributions can not be easily separated. Thus this 'vertical disc–halo conspiracy' is much like the classical disc–halo conspiracy which arises in considerations of the radial distribution of luminous and dark luminous matter derived from galaxy rotation curves.

From the data presented in Table A1 it is clear that, without additional assumptions, stellar kinematical data extending to a few hundred parsecs are not sufficient to determine the mass of the stellar disc. However, $\Sigma_{\rm tot}^{1.1}$ is much better determined (rightmost column of Table A1), in agreement with KG91. In order to discriminate between models, it is essential to incorporate a rotation curve constraint to limit the possible DM densities. KG89b used such a constraint explicitly, while Bahcall (1984b) and Flynn & Fuchs (1994) used 'reasonable' values for the density of non-disc-like DM to rule out extreme values for the mass of the stellar disc. Furthermore, if data at larger z are considered, the differences between the force laws shown in Fig. A1 start to become apparent and can be used to limit the allowed range for Σ_* (Flynn & Fuchs 1994).

Although the model parameters we have used to construct Fig. A1 and Table A1 lie at the extreme end of the models investigated by KG89b and KG91, we find that other models, within the 1–2σ range of Θ_0/R_0, $h_{\rm d}$, Σ_* and $\Sigma_{\rm tot}^{1.1}$, yield similar results. Thus, mass models for the Milky Way *have* to conform to the constraint $\Sigma_{\rm tot}^{1.1} = (71 \pm 6)\,M_\odot\,pc^{-2}$. To summarize the above, in order to determine the stellar column density from stellar kinematics, the existence of the vertical disc–halo conspiracy requires that one *has* to include self-consistent rotation curve constraints and/or sample the region above 800 pc.

[10] For the ensemble of models for which the parameters differ by $\leq 1\sigma$ from the model presented here, the approximations based on equation (A1) reproduce the true K_z typically to within 7 per cent: sometimes models that include the rotation curve gradient term perform best, sometimes not. The same is true for the models listed in Table 2 with other Galactic constants than those presented in Fig. A1.

APPENDIX B: STELLAR KINEMATICS AND THE RELATION BETWEEN THE MODEL'S PARAMETERS

In Section 3.2 we described how the observationally determined $\Sigma_{\rm tot}^{1.1}$ – value imposes correlations between luminous and dark matter in the solar neighbourhood. In this section we present some specific examples to illustrate what we can learn about the structure of the Milky Way by treating Σ_* as a parameter which is only constrained by $\Sigma_{\rm tot}^{1.1}$ (cf. equation 5). Note that these correlations are independent of any H I flaring constraints.

At the solar circle, and for $z = 1.1$ kpc, equation (4) can be rearranged to read:

$$\frac{\Sigma_{\rm h}^{1.1}(q)}{\Sigma_{\rm h}^{1.1}(1)} \approx 1.1R_0 + R_0(0.9 - R_0)q \quad q \lesssim 0.15 \qquad \text{(B1)}$$

$$\approx q^{-13/20}, \qquad q \gtrsim 0.15, \qquad \text{(B2)}$$

where the core radius has been set to R_0. In this appendix we use – for the sake of convenience – the symbol q for the halo flattening derived from the local stellar kinematics constraint, and $q_{\rm H\,I}$ for the halo's shape derived from the H I flaring. Taking the fiducial values for $\Sigma_{\rm tot}^{1.1}$, Σ_* and $\Sigma_{\rm g}$ to be 71, 35 and $14.5\,M_\odot\,pc^{-2}$, respectively, and employing equation (5), we determine the fiducial value for $\Sigma_{\rm h}^{1.1}$ to be $21.5\,M_\odot\,pc^{-2}$. Further, defining $\Sigma_* = 35 + \delta\Sigma_*$, using the fiducial columndensities defined above, and applying equations (B1) and (B2), we can relate the required halo flattening to $\delta\Sigma_*$:

$$q \approx \frac{21.5 - R_0\Sigma_{\rm h}^{1.1}(1) - \delta\Sigma_*}{0.9R_0^2\Sigma_{\rm h}^{1.1}(1)} \qquad \text{(B3)}$$

$$\approx \left(\frac{\Sigma_{\rm h}^{1.1}(1)}{21.5}\right)^{20/13}\left[1 + \left(\frac{20/13}{21.5}\right)\delta\Sigma_*\right] \qquad \text{(B4)}$$

for the same q-ranges as in equations (B1) and (B2). Since $\Sigma_{\rm h}^{1.1}(q = 1)$ depends on Θ_0 (equation 4), the solutions of equations (B3) and (B4) depend on R_0, Θ_0 and $\delta\Sigma_*$. We use our mass models to determine $\Sigma_{\rm h}^{1.1}(q = 1; R_0, \Theta_0)$, and rewrite equations (B3) and (B4) for a few interesting cases. For $\delta\Sigma_* = 0$ we find:

$$q \approx 0.07 \pm 0.05 \qquad (\Theta_0 = 165) \qquad \text{(B5)}$$

$$q \approx 0.4 - 0.1(R_0 - 7.1) \pm 0.1 \qquad (\Theta_0 = 175) \qquad \text{(B6)}$$

$$q \approx 0.8 - 0.2(R_0 - 7.1) \pm 0.2 \qquad (\Theta_0 = 185), \qquad \text{(B7)}$$

Thus, lower rotation speeds and larger R_0s require more highly flattened haloes. Furthermore, for any fixed value of R_0, the *slope* of the $q - \delta\Sigma_*$ relation depends strongly upon Θ_0. For example, with $R_0 = 7.1$ kpc we find:

$$q \approx 0.069 + 0.005\delta\Sigma_* \qquad (\Theta_0 = 165) \qquad \text{(B8)}$$

$$q \approx 0.400 + 0.030\delta\Sigma_* \qquad (\Theta_0 = 175) \qquad \text{(B9)}$$

$$q \approx 0.800 + 0.060\delta\Sigma_* \qquad (\Theta_0 = 185). \qquad \text{(B10)}$$

Equations (B5) to (B10) clearly show that small values of the Galactic rotation speed imply a highly flattened dark matter halo,

whatever our distance to the Galactic Centre, and whatever the mass of the stellar disc. We also see that the last relations constrain Σ_* rather tightly: for models with $\Theta_0 \sim 185(175)\,\mathrm{km\,s^{-1}}$, an increase in the stellar column density of $\sim 3(20)\,\mathrm{M_\odot\,pc^{-2}}$ covers the whole allowed range for q.

In Section 4.4 and Fig. 2 we have seen that the stellar kinematics and H I flaring constraints provide mutually exclusive constraints on Σ_* and q if both the rotation speed and the effective velocity dispersion are small. This can be understood as follows: equations (B5)–(B10) show that the $\Sigma^{1.1}_{\rm tot}$ constraint implies small q-values for low Θ_0s. Likewise, the H I flaring constraint yields small qs for small Θ_0s, but only if the velocity dispersion does not decrease by too much (cf. equation 16). Furthermore, because the slope of the $q(\Sigma_*)$ relation becomes shallower with decreasing Θ_0, the accessible range for $q_{1.1}$ decreases with Θ_0. If the flaring analysis leads to a $q_{\rm H\,I} \sim 1$ halo, extreme values for Σ_* are required to match $q_{1.1}$ with $q_{\rm H\,I}$. Obviously, if the required stellar column exceeds $\Sigma^{1.1}_{\rm tot}$, it is not possible to construct a self-consistent model for that particular combination of Galactic constants and gaseous velocity dispersion. In these circumstances it is possible that our procedure to determine Σ_* and q yields extreme values for Σ_* and q, and sometimes even negative values.

APPENDIX C: ERROR ESTIMATION

At this point it is also possible to estimate the accuracy to which the various parameters in Fig. 2 are determined. For example, as we have seen before, the halo flattening inferred from the H I flaring has only a slight dependency on the mass of the stellar disc (cf. fig. 3 of Paper I). This allows us to estimate the flattening of the halo by averaging the $q_{\rm H\,I}$ values from the various model runs at a given R_0 and Θ_0. For example, the nine $q_{\rm H\,I}$ errors tabulated in Table 2 yield $\delta q_{\rm H\,I}/q_{\rm H\,I} \sim 0.06$ for the two low R_0 values at $q \sim 0.7$ Employing $q \propto \Theta_0^2$ (cf. equation 17), we find:

$$\frac{\delta\Theta_0}{\Theta_0} \sim \frac{\delta q_{\rm H\,I}}{2q_{\rm H\,I}}. \tag{C1}$$

The $q_{\rm H\,I}$ values as determined from the flaring measurements are thus precise to about 6, while the value of the local Galactic rotation speed we derive from $q_{\rm H\,I}$ measurement has an estimated accuracy of 3 per cent.

To estimate how well the local stellar column density is determined from the flaring and the observed $\Sigma^{1.1}_{\rm tot}$ value of the total column density, we rewrite equation (B4) to read $q = c_1(1 + c_2\delta\Sigma_*)$, and find:

$$\delta(\delta\Sigma_*) \sim \frac{q}{c_1 c_2}\sqrt{\left(\frac{\delta q}{q}\right)^2 + \left(\frac{\delta c_1}{c_1}\right)^2}, \tag{C2}$$

where $c_1 = \Sigma^{1.1}_{\rm h}(1)/21.5$, $c_2 = (20/13)/21.5$ and $q/(c_1c_2) \sim 11.2$ for $q = 0.8$ and $\Sigma^{1.1}_{\rm h}(1) = 21.5$. If assume that c_1 is without error, the second term in equation (C2) vanishes, and we arrive at a lower limit for the error in Σ_* of about $0.7\,\mathrm{M_\odot\,pc^{-2}}$. If we assign the full error in the observed total column density ($6\,\mathrm{M_\odot\,pc^{-2}}$) to $\Sigma^{1.1}_{\rm h}(1)$, we have $c_1 \sim 1 \pm 0.43$, so that $\delta(\delta\Sigma_*) = 11.2\sqrt{(0.06)^2 + (0.43)^2} \sim 4.8\,\mathrm{M_\odot\,pc^{-2}}$. We thus estimate that our method of deriving the stellar column density has an accuracy somewhere between 0.7 and $4.8\,\mathrm{M_\odot\,pc^{-2}}$ or about to 2 to 14 per cent.

The error estimates above are close to the errors derived from our detailed modelling procedure.

Table D1. The surface density and thickness of the atomic and molecular hydrogen components in the Milky Way as a function of scaled Galactocentric radius, R/R_0. The H I and H_2 columndensities have units $\mathrm{M_\odot\,pc^{-2}}$. The widths listed are full-widths at half-maximum (FWHM) and have units of R_0. For $R > R_0$, the widths of the H I layer is the average of several works; see Paper I for details. Some entries have been left blank: we were unable to derive reliable widths at these radii. The columndensities at these radii are from Wouterloot et al. (1990).

R/R_0	$\Sigma_{\rm H\,I}$	$\Sigma_{\rm H_2}$	$W_{\rm H\,I}$	$\delta W_{\rm H\,I}$	$W_{\rm H_2}$
0.218	0.59	1.08	0.0330	0.0014	0.0151
0.276	1.04	1.54	0.0320	0.0031	0.0158
0.309	1.23	1.47	0.0323	0.0017	0.0134
0.343	1.30	1.67	0.0306	0.0014	0.0119
0.376	1.29	2.67	0.0294	0.0008	0.0131
0.409	1.31	4.29	0.0268	0.0045	0.0140
0.440	1.41	4.91	0.0290	0.0031	0.0142
0.467	1.59	5.02	0.0313	0.0028	0.0143
0.499	1.85	5.57	0.0278	0.0011	0.0153
0.530	2.10	6.23	0.0240	0.0017	0.0165
0.559	2.30	5.87	0.0301	0.0014	0.0168
0.586	2.48	5.48	0.0346	0.0014	0.0163
0.612	2.90	5.18	0.0344	0.0023	0.0152
0.641	3.72	4.62	0.0415	0.0034	0.0139
0.668	4.36	3.94	0.0504	0.0017	0.0129
0.692	4.24	3.73	0.0525	0.0014	0.0120
0.717	3.60	3.97	0.0447	0.0031	0.0115
0.742	3.17	4.27	0.0452	0.0039	0.0122
0.764	3.23	4.33	0.0485	0.0130	0.0136
0.786	3.68	4.09	0.0495	0.0101	0.0152
0.806	4.22	3.60	0.0565	0.0039	0.0161
0.828	4.72	2.95	0.0530	0.0048	0.0159
0.848	4.90	2.44	0.0570	0.0034	0.0144
0.865	4.80	2.06	0.0572	0.0011	0.0134
0.882	4.52	1.70	0.0509	0.0014	0.0136
0.897	4.41	1.45	0.0525	0.0020	0.0146
0.913	4.75	1.30	0.0523	0.0036	0.0158
0.926	5.39	1.26	0.0652	0.0017	0.0167
0.938	6.13	1.29	0.0730	0.0020	0.0174
1.000	9.25	1.80	0.0577	0.0042	0.0199
1.058	8.57	1.80			
1.089	7.77	1.28	0.0611	0.0044	0.0238
1.193	6.09	0.44			
1.332	6.56	1.62	0.0734	0.0061	0.0385
1.457	7.45	1.47			
1.586	7.62	1.10	0.0801	0.0062	0.0458
1.721	6.02	0.54			
1.848	5.30	0.37	0.1108	0.0099	0.0742
1.995	4.36	0.20			
2.101	3.41	0.11	0.1391	0.0115	0.0767
2.177	3.31	0.14			
2.262	2.84	0.12			
2.355	2.36	0.09	0.1666	0.0143	
2.443	2.01	0.05			
2.532	1.66	0.01			

APPENDIX D: THE ISM OF THE MILKY WAY TABULATED

In this appendix we present a tabulated version of the radial variation of the atomic and molecular hydrogen, as well as their widths (Table D1). We present these data in a manner which is *independent* of the values of the Galactic constants as well as the shape of the rotation curve. The H I column density at the solar circle position includes $1.4\,\mathrm{M_\odot\,pc^{-2}}$ of ionized hydrogen. No ionized hydrogen is included at any other radius. The column

densities listed do not include the contribution due to helium. In our model calculations of the potential we increase the listed column densities to include 23.8 per cent helium. We have brought the data from the sources listed in Section 2.1 on to a common distance scale defined by Merrifield's (1992) determination of the $W(R/R_0) = v_{rad}/(\sin\ell\cos b)$ curve. Here v_{rad} and ℓ and b are the radial velocity and the Galactic coordinates, respectively. In practice, this rescaling works as follows: (1) from the rotation curve $[\Theta'(R')]$ in the original reference, determine R'/R'_0 and $W'(R'/R'_0) \equiv R'_0[\Theta'(R')/R' - \Theta'_0/R'_0]$ (the primed quantities refer to the values assumed in the reference), (2) for each property X' (gas-layer width and volume density), determine $X'(W')$ from $X'(R')$ and $W'(R')$, (3) find Merrifield's R/R_0 values for which $W = W'$, and (4) the property X' re-gridded on to Merrifield's distance scale is now given by $X(R/R_0)$.

This paper has been typeset from a TEX/LATEX file prepared by the author.